

Efficient implementation and performance evaluation of the Wigner branching random walk

Yunfeng Xiong Sihong Shao^{†,*}

January 2, 2022

Abstract

To implement the Wigner branching random walk, the particle carrying a signed weight, either -1 or $+1$, is more friendly to data storage and arithmetic manipulations than that taking a real-valued weight continuously from -1 to $+1$. The former is called a signed particle and the latter a weighted particle. The existed signed-particle implementation is indeed a special case of the weighted-particle one by choosing a non-constant auxiliary function, but it poses a restriction on the time step. In this paper, we propose two efficient strategies to realize the signed-particle implementation, which utilizes a constant auxiliary function and allows the use of a longer time step. One is to interpret the multiplicative functional as the probability to generate pairs of particles instead of the incremental weight, and the other is to utilize a bootstrap filter to adjust the skewness of particle weights. Performance evaluations on the Gaussian barrier scattering (2D) and a Helium-like system (4D) demonstrate the feasibility of both strategies. Details on implementing the importance sampling according to the quasi-probability density and an efficient resampling or particle reduction are provided.

AMS subject classifications: 60J85; 81S30; 45K05; 65M75; 82C10; 81V70; 81Q05

Keywords: Wigner equation; branching random walk; signed particle; Monte Carlo method; resampling; bootstrap filtering; weighted particle

1 Introduction

The Wigner function $f(\mathbf{x}, \mathbf{k}, t)$ for a N -body d -dimensional quantum system lives in the phase space $(\mathbf{x}, \mathbf{k}) \in \mathbb{R}^{2n}$ with $n = Nd$ for position \mathbf{x} and wavevector \mathbf{k} , and satisfies the following Wigner equation (WEQ) [1]

$$\frac{\partial}{\partial t} f(\mathbf{x}, \mathbf{k}, t) + \frac{\hbar \mathbf{k}}{m} \cdot \nabla_{\mathbf{x}} f(\mathbf{x}, \mathbf{k}, t) = \int_{\mathbb{R}^n} d\mathbf{k}' f(\mathbf{x}, \mathbf{k}', t) V_w(\mathbf{x}, \mathbf{k} - \mathbf{k}', t), \quad (1.1)$$

[†]LMAM and School of Mathematical Sciences, Peking University, Beijing 100871, China.

*To whom correspondence should be addressed. Email: sihong@math.pku.edu.cn

where the Wigner kernel V_w reads

$$V_w(\mathbf{x}, \mathbf{k}, t) = \frac{1}{i\hbar(2\pi)^n} \int_{\mathbb{R}^n} d\mathbf{y} e^{-i\mathbf{k}\cdot\mathbf{y}} \left[V\left(\mathbf{x} + \frac{\mathbf{y}}{2}, t\right) - V\left(\mathbf{x} - \frac{\mathbf{y}}{2}, t\right) \right]. \quad (1.2)$$

Here \hbar is the reduced Planck constant, \mathbf{k}/\mathbf{m} is short for $(\mathbf{k}_1/m_1, \dots, \mathbf{k}_N/m_N)$ and m_i is the mass of the i -th body. In the past few decades, WEQ has been drawing a growing attention, especially in the simulations of nanodevices [2, 3] as well as the many-body quantum mechanics [4, 5], due to its theoretical advantage [6, 7].

The huge challenge to the numerical resolution of WEQ lies in the high dimensionality of the phase space, which are unfriendly to traditional deterministic solvers. A class of stochastic algorithms has recently been proposed and its mathematical theory consists of three components: the probabilistic interpretation of WEQ, the principle of importance sampling and the technique of density estimation [5, 8]. The corresponding implementations borrow several fundamental concepts from the direct simulation Monte Carlo method for the Boltzmann equation, including particle weights, random jumps and particle cancellations [9–11]. In this manner, it paves a promising way to overcome the curse of dimensionality, and several benchmarks have also revealed its reliability in capturing fine structures of 2D and 4D quantum systems [5, 12, 13].

Although all Monte Carlo approaches almost rely on the equivalent stochastic interpretation of WEQ, there exist significant differences among various realizations and thereby resulting in distinct performances. The original signed particle Wigner Monte Carlo method (abbreviated as **sp0**) is suggested to choose a variable auxiliary function $\gamma(\mathbf{x})$ and confine the particle weights to either +1 or -1 (termed the signed particle) [9, 14]. Such setting greatly facilitates the data storage and the arithmetic operation, but poses a limitation on the time step in order to maintain the accuracy. In our previous work [5], we have proposed the Wigner branching random walk (WBRW) model, in which the multiplicative functionals are interpreted as the importance weights, yielding the weighted-particle branching random walk algorithm (abbreviated as **wp**). Simulating the WBRW ameliorates the restriction on the time step and allows a reduction in variance by choosing a large constant $\gamma(\mathbf{x})$. The price to pay is that particle weights have to take values continuously in $[-1, 1]$ (termed the weighted particle). As a special case, **sp0** is fully recovered from **wp** by choosing an auxiliary function according to the Wigner kernel V_w . But a constant auxiliary function $\gamma(\mathbf{x}) \equiv \gamma_0$ is much more preferable when simulating actual many-body quantum systems.

This paper intends to discuss another two efficient strategies to implement WBRW. The performance of stochastic methods is usually related to the variance reduction, data storage, as well as an appropriate choice of particle size N_α . Therefore, our goals are to get both advantages of **sp0** and **wp**, say, the setting of signed weights and the manner to improve the accuracy systematically. Besides, we will discuss the criterion to choose an appropriate particle size, which may be related to both the accuracy of the Monte Carlo simulations and the efficiency of the resampling techniques. First, the signed-particle branching random walk algorithm (abbreviated as **sp1**) is proposed, where the multiplicative functional is interpreted as the

probability to generate pairs of particles and thus the particle weights are confined to be either 1 or -1. However, numerical experiments demonstrate that the variance of **sp1** is usually larger than that of **wp** and cannot be diminished by increasing $\gamma(\mathbf{x})$. To save it, we introduce a bootstrap filter in **wp** to adjust particle weights to ± 1 and preserve the variance reduction property, yielding another signed-particle implementation (abbreviated as **sp2**). A theoretical error bound on the bootstrap filtering is analyzed and ensures the convergence as $N_\alpha \rightarrow \infty$. Detailed performance evaluations demonstrate the convergence, accuracy and efficiency of the proposed strategies, with the reference solutions produced by several highly accurate deterministic solvers [15, 16]. For resampling, it is observed that the particle size should be comparable to the partition size if a uniform histogram is adopted, otherwise both efficiency and accuracy are undermined. In fact, similar phenomena have also been reported in statistical community, referring to the current challenge to the multivariate density estimation (particle cancelation) [17, 18].

The remaining of this paper is organized as follows. In Section 2, we briefly review the mathematical theory of the WBRW. Two strategies of the signed-particle implementation are given in Section 3, and several important issues on the implementation are illustrated in Section 4. For the sake of readers' convenience, we try our best to illustrate all the details and unfold the 'blackbox' of coding WBRW. A sequence of performance evaluations is reported in Section 5, which makes a thorough comparison among **sp1**, **sp2** and **wp**, as well as **sp0**. The conclusions are drawn in Section 6.

2 The Wigner branching random walk

The mathematical framework for exploring the inherent relation between the WBRW and the WEQ has been established recently from the viewpoint of computational mathematics [5]. For the sake of completeness as well as readers' convenience, we will give a brief overview of the main findings there in this section and assume that the potential in Eq. (1.2) is time-independent for brevity hereafter.

To connect rigorously the WBRW to Eq. (1.1), an auxiliary function $\gamma(\mathbf{x})$ is added on both sides of Eq. (1.1) in an equivalent manner for producing the exponential distribution, and then the resulting equation can be cast into a renewal-type integral equation

$$f(\mathbf{x}, \mathbf{k}, t) = [1 - \mathcal{H}(0; \mathbf{x}, t)] f(\mathbf{x}(t), \mathbf{k}, 0) + \int_0^t d\mathcal{H}(t'; \mathbf{x}, t) \int_{\mathbb{R}^n} d\mathbf{x}' \int_{\mathcal{K}} d\mathbf{k}' \frac{\Gamma(\mathbf{x}(t-t'), \mathbf{k}; \mathbf{x}', \mathbf{k}')}{\gamma(\mathbf{x}(t-t'))} f(\mathbf{x}', \mathbf{k}', t'), \quad (2.1)$$

where

$$\mathcal{H}(t'; \mathbf{x}, t) = \int_{t'}^t \gamma(\mathbf{x}(t-\tau)) e^{-\int_\tau^t \gamma(\mathbf{x}(t-s)) ds} d\tau \quad (2.2)$$

is a probability measure with respect to t' for a given (\mathbf{x}, t) on $t' \leq t$ provided that

the auxiliary function $\gamma(\mathbf{x})$ satisfies

$$\gamma(\mathbf{x}) \geq 0, \quad \lim_{t' \rightarrow -\infty} \int_{t'}^t \gamma(\mathbf{x}(t-s)) ds = +\infty, \quad \forall \mathbf{x} \in \mathbb{R}^n, \quad (2.3)$$

$\mathbf{x}(\Delta t) = \mathbf{x} - \hbar \mathbf{k} \Delta t / \mathbf{m}$ denotes the backward-in-time trajectory of (\mathbf{x}, \mathbf{k}) with a positive time increment Δt . It's readily seen from Eq. (2.1) that $\gamma(\mathbf{x})$ serves as the intensity of an exponential distribution. The kernel $\Gamma(\mathbf{x}, \mathbf{k}; \mathbf{x}', \mathbf{k}')$ is given by

$$\Gamma(\mathbf{x}, \mathbf{k}; \mathbf{x}', \mathbf{k}') = [V_w^+(\mathbf{x}, \mathbf{k} - \mathbf{k}') - V_w^-(\mathbf{x}, \mathbf{k} - \mathbf{k}') + \gamma(\mathbf{x})\delta(\mathbf{k} - \mathbf{k}')] \delta(\mathbf{x} - \mathbf{x}'), \quad (2.4)$$

and we have adopted the k -truncated Wigner kernel for the purpose of numerical computation, namely, the \mathbf{k} -space is truncated into a finite domain \mathcal{K} and a simple nullification adopted outside \mathcal{K} by exploiting the decay of the Wigner function when $|\mathbf{k}| \rightarrow +\infty$ due to the Riemann-Lebesgue lemma.

Splitting the Wigner kernel into positive and negative parts in (2.4) is of great importance to a probabilistic interpretation. In general, the Wigner kernel V_w is composed of M parts $V_w = V_{w,1} + V_{w,2} + \dots + V_{w,M}$, that corresponds to the potential $V = V_1 + V_2 + \dots + V_M$, then the Wigner kernel can be split into M pairs as follows

$$V_w = V_w^+ - V_w^-, \quad V_w^\pm = \sum_{i=1}^M V_{w,i}^\pm, \quad V_{w,i}^\pm = \frac{1}{2} |V_{w,i}| \pm \frac{1}{2} V_{w,i}. \quad (2.5)$$

Such setting is also very helpful in dealing with complicated systems composed of two-body interactions, as combining it with the Fourier completeness relation helps to decompose the convolution term in Eq. (1.1) into several lower dimensional integrals, for instance, see Example 1.

Example 1. We consider a 4D Helium-like system, in which the potential is composed of electron-nucleus attractive Yukawa interactions and electron-electron repulsive Yukawa interaction,

$$\begin{aligned} V(x_1, x_2) &= V_{\text{ne}}(x_1) + V_{\text{ne}}(x_2) + V_{\text{ee}}(x_1, x_2) \\ &= -\frac{2e^{-\kappa|x_1-x_A|}}{2\kappa} - \frac{2e^{-\kappa|x_2-x_A|}}{2\kappa} + \frac{e^{-\kappa|x_1-x_2|}}{2\kappa}. \end{aligned} \quad (2.6)$$

The parameter κ expresses the screening strength, x_A denotes the position of the nucleus, and $x_i (i = 1, 2)$ is the position of the i -th electron. The corresponding Wigner kernel reads

$$V_{w,\text{ne}}(x_i, k_i) = -\frac{2}{\hbar\pi} \cdot \frac{\sin(2k_i(x_i - x_A))}{4k_i^2 + \kappa^2}, \quad (2.7)$$

$$V_{w,\text{ee}}(x_1, x_2, k_1, k_2) = \frac{4}{\hbar\pi} \cdot \frac{\sin(2k_1x_1 + 2k_2x_2)}{|k_1 - k_2|^2 + \kappa^2} \cdot \delta(2k_1 + 2k_2). \quad (2.8)$$

As a result, the convolution term is decomposed into three 1D integrals:

$$\int_{\mathbb{R}^2} V_w(\mathbf{x}, \mathbf{k} - \mathbf{k}') f(\mathbf{x}, \mathbf{k}', t) d\mathbf{k}' = I_1(\mathbf{x}, \mathbf{k}, t) + I_2(\mathbf{x}, \mathbf{k}, t) + I_3(\mathbf{x}, \mathbf{k}, t), \quad (2.9)$$

$$I_1(\mathbf{x}, \mathbf{k}, t) = -\frac{2}{\hbar\pi} \int_{\mathbb{R}} \frac{\sin(2k' \cdot (x_1 - x_A))}{4(k')^2 + \kappa^2} f(x_1, x_2, k_1 - k', k_2, t) dk', \quad (2.10)$$

$$I_2(\mathbf{x}, \mathbf{k}, t) = -\frac{2}{\hbar\pi} \int_{\mathbb{R}} \frac{\sin(2k' \cdot (x_2 - x_A))}{4(k')^2 + \kappa^2} f(x_1, x_2, k_1, k_2 - k', t) dk', \quad (2.11)$$

$$I_3(\mathbf{x}, \mathbf{k}, t) = \frac{1}{\hbar\pi} \int_{\mathbb{R}} \frac{\sin(2k' \cdot (x_1 - x_2))}{4(k')^2 + \kappa^2} f(x_1, x_2, k_1 - k', k_2 + k', t) dk'. \quad (2.12)$$

The main use of the Wigner function is to calculate observables $\langle \hat{A} \rangle_T$ at a given final time T , such as the averaged position of particles, electron density, etc., all of which involve the inner product problem

$$\langle g_0, f \rangle = \int_0^T dt \int_{\mathbb{R}^n} d\mathbf{x} \int_{\mathcal{K}} d\mathbf{k} g_0(\mathbf{x}, \mathbf{k}, t) f(\mathbf{x}, \mathbf{k}, t). \quad (2.13)$$

In consequence, we have

$$\langle \hat{A} \rangle_T = \langle g_0, f \rangle \quad \text{and} \quad g_0(\mathbf{x}, \mathbf{k}, t) = A(\mathbf{x}, \mathbf{k}) \delta(t - T). \quad (2.14)$$

Here $\hat{A}(\hat{\mathbf{x}}, \hat{\mathbf{k}})$ is an arbitrary quantum operator, and $A(\mathbf{x}, \mathbf{k})$ the corresponding Weyl symbol. Actually, the WBRW algorithms are devoted into estimating $\langle \hat{A} \rangle_T$ and bottomed on the dual theory of WEQ. It has been proved that the average value $\langle \hat{A} \rangle_T$ can be determined *only by the 'initial' data* as follows

$$\langle \hat{A} \rangle_T = \int_{\mathbb{R}^n} d\mathbf{x} \int_{\mathcal{K}} d\mathbf{k} f(\mathbf{x}, \mathbf{k}, 0) \varphi(\mathbf{x}, \mathbf{k}, 0), \quad (2.15)$$

where the dual variable $\varphi(\mathbf{x}, \mathbf{k}, t)$ satisfies

$$\begin{aligned} \varphi(\mathbf{x}, \mathbf{k}, t) &= [1 - \mathcal{G}(T; \mathbf{x}, t)] A(\mathbf{x}(T - t), \mathbf{k}) \\ &+ \int_t^T d\mathcal{G}(t'; \mathbf{x}, t) \int_{\mathbb{R}^n} d\mathbf{x}' \int_{\mathcal{K}} d\mathbf{k}' \frac{\Gamma(\mathbf{x}', \mathbf{k}'; \mathbf{x}(t' - t), \mathbf{k})}{\gamma(\mathbf{x}(t' - t))} \varphi(\mathbf{x}', \mathbf{k}', t'). \end{aligned} \quad (2.16)$$

Eq. (2.16) can be regarded as the dual correspondence of Eq. (2.1). Noting that it is required $t' \geq t$ for convenience in the former, but $t' \leq t$ is always assumed in the latter. Here,

$$\mathcal{G}(t'; \mathbf{x}, t) = \int_t^{t'} \gamma(\mathbf{x}(\tau - t)) e^{-\int_t^\tau \gamma(\mathbf{x}(s-t)) ds} d\tau \quad (2.17)$$

is again a probability measure with respect to t' for given (\mathbf{x}, t) on $t' \geq t$ under the assumption that the auxiliary function satisfies

$$\gamma(\mathbf{x}) \geq 0, \quad \lim_{t' \rightarrow +\infty} \int_t^{t'} \gamma(\mathbf{x}(t - s)) ds = +\infty, \quad \forall \mathbf{x} \in \mathbb{R}^n, \quad (2.18)$$

and $\mathbf{x}(\Delta t) = \mathbf{x} + \hbar \mathbf{k} \Delta t / \mathbf{m}$ denotes the forward-in-time trajectory of (\mathbf{x}, \mathbf{k}) with a positive time increment Δt .

The reasons why we mainly focus on the adjoint equation, instead of the original WEQ, are as two-fold. First, Eq. (2.15) allows the use of the importance sampling approach, with $f_I \propto |f(\mathbf{x}, \mathbf{k}, 0)|$ chosen as the instrumental distribution. Second, estimating $\varphi(\mathbf{x}, \mathbf{k}, 0)$ can be implemented in a time-marching manner. By contrast, the backward-in-time stochastic algorithms are pointwise in nature and only attractive when one is interested in estimating only a few values of $f(\mathbf{x}, \mathbf{k}, t)$ [19].

A branching random walk model has been introduced in [5] with its expectation consistent with the mild solution of the adjoint equation (2.16). In the branching particle system, particles carrying importance weights are indexed by a branching random tree, and their motions are described by deterministic travels and random jumps (no diffusions are involved). We summarize the rules of the branching particle system in Alg. 1, and the implementations are resorted to the sequential Monte Carlo techniques [20].

Our ultimate goal is to derive the following estimator $\langle \hat{A} \rangle_{t_l, t_{l+1}}$, where t_l and t_{l+1} denote the initial and final instant, respectively.

$$\langle \hat{A} \rangle_{t_l, t_{l+1}} \approx \frac{1}{N_\alpha} \sum_{\alpha} \sum_{j \in \mathcal{E}_\alpha} \varphi(\mathbf{x}_{j,\alpha}, \mathbf{k}_{j,\alpha}, t_l) \cdot w_{j,\alpha}(t_l) = \langle A, \frac{1}{N_\alpha} \sum_{i=1}^N w_i \delta_{\mathbf{x}_i, \mathbf{k}_i} \rangle. \quad (2.23)$$

Here N_α is the particle size, the indices $\alpha \in \{1, \dots, N_\alpha\}$ mark the draws (particles) from the instrumental probability density f_I and the index set \mathcal{E}_α marks the offsprings produced by α -th particle, and the equality is only a rearrangement of the indices. For more details, one can refer to [5].

3 Signed-particle WBRW: two strategies

The major difference between **wp** and **sp1** is attributed to the probabilistic interpretation of the multiplicative functional $\xi_m(\mathbf{x})/\gamma(\mathbf{x})$ (we use ξ/γ for brevity), which is treated as the weight function in the former and the probability to generate particles in the latter. On the other hand, **sp2** is essentially a weighted-particle implementation, but associated with a bootstrap filtering to adjust the continuous weights into signed weights, as illustrated in Alg. 2. The bootstrap filtering provides a useful way to adjust the skewness of particle weights, but usually requires weight functions to be positive semidefinite. Here we will extend the theory to deal with particles carrying weights in $[-1, 1]$.

3.1 The choice of $\gamma(\mathbf{x})$

Before proceeding, we need to review the choice of $\gamma(\mathbf{x})$ in **sp0**. It suggests that V_w is split into positive and negative parts (namely, $M = 1$), and the auxiliary function is nothing but the normalizing factor $\xi(\mathbf{x})$ [9, 21]:

$$\gamma(\mathbf{x}) = \xi(\mathbf{x}) = \int_{2\mathcal{K}} V_w^+(\mathbf{x}, \mathbf{k}) d\mathbf{k}, \quad (3.1)$$

Algorithm 1 Rules of the Wigner branching random walk

Suppose each particle in the branching particle system, carrying an initial weight either 1 or -1 , starts at state $(\mathbf{x}_\alpha, \mathbf{k}_\alpha)$ at time t_l and moves until $t_{l+1} = t_l + \Delta t$ according to the following rules.

1. The particle at $(\mathbf{x}, \mathbf{k}, t)$ dies in the age time interval $(t, t') \subset [t_l, t_{l+1}]$ with probability $1 - \int_t^{t+\tau} e^{-\gamma(\mathbf{x}(s-t))} ds$, with a random life-length $\tau = t' - t$.
2. If $t + \tau \geq t_{l+1}$, say, the life-length of the particle exceeds $t_{l+1} - t$, the particle immigrates to the state $(\mathbf{x}(t_{l+1} - t), \mathbf{k})$ and becomes frozen.
3. If $t + \tau < t_{l+1}$, the particle carrying the weight w dies at age $t' = t + \tau$ at state $(\mathbf{x}(\tau), \mathbf{k})$ and produces at most $2M + 1$ offsprings at states $(\mathbf{x}'_{(1)}, \mathbf{k}'_{(1)})$, \dots , $(\mathbf{x}'_{(2M+1)}, \mathbf{k}'_{(2M+1)})$, endowed with updated weights $w_{(1)}, \dots, w_{(2M+1)}$.

$$\mathbf{x}'_{(1)} = \mathbf{x}'_{(2)} = \dots = \mathbf{x}'_{(2M+1)} = \mathbf{x}(\tau) = \mathbf{x} + \frac{\hbar \mathbf{k} \tau}{\mathbf{m}}, \quad (2.19)$$

$$\mathbf{k} - \mathbf{k}'_{(2m-1)} \propto \frac{V_{w,m}^-(\mathbf{x}(\tau), \mathbf{k})}{\xi_m(\mathbf{x}(\tau))}, \quad \mathbf{k} - \mathbf{k}'_{(2m)} \propto \frac{V_{w,m}^+(\mathbf{x}(\tau), \mathbf{k})}{\xi_m(\mathbf{x}(\tau))}, \quad (2.20)$$

$$\mathbf{k}'_{(2M+1)} = \mathbf{k}, \quad (2.21)$$

$$\xi_m(\mathbf{x}) = \int_{2\mathcal{K}} V_{w,m}^+(\mathbf{x}, \mathbf{k}) d\mathbf{k} = \int_{2\mathcal{K}} V_{w,m}^-(\mathbf{x}, \mathbf{k}) d\mathbf{k}. \quad (2.22)$$

For **sp1**, the i -th offspring is generated with probability $\Pr_{(i)}$.

$$\Pr_{(2m-1)} = \xi_{2m-1}(\mathbf{x}(\tau)) \cdot \gamma(\mathbf{x}(\tau))^{-1} \cdot \mathbb{1}_{\{\mathbf{k}'_{2m-1} \in \mathcal{K}\}}, \quad \Pr_{(2M+1)} = 1,$$

$$\Pr_{(2m)} = \xi_{2m}(\mathbf{x}(\tau)) \cdot \gamma(\mathbf{x}(\tau))^{-1} \cdot \mathbb{1}_{\{\mathbf{k}'_{2m} \in \mathcal{K}\}},$$

$$w_{(2m-1)} = w, \quad w_{(2m)} = -w, \quad w_{(2M+1)} = w.$$

For **sp2** and **wp**, the i -th offspring is generated with probability 1.

$$w_{(2m-1)} = \xi_{2m-1}(\mathbf{x}(\tau)) \cdot \gamma(\mathbf{x}(\tau))^{-1} \cdot \mathbb{1}_{\{\mathbf{k}'_{2m-1} \in \mathcal{K}\}} \cdot w, \quad w_{(2M+1)} = w,$$

$$w_{(2m)} = \xi_{2m-1}(\mathbf{x}(\tau)) \cdot \gamma(\mathbf{x}(\tau))^{-1} \cdot \mathbb{1}_{\{\mathbf{k}'_{2m} \in \mathcal{K}\}} \cdot w.$$

For **sp0**, $M = 1$ and the i -th offspring is generated with probability 1.

$$w_{(1)} = \mathbb{1}_{\{\mathbf{k}'_1 \in \mathcal{K}\}} \cdot w, \quad w_{(2)} = \mathbb{1}_{\{\mathbf{k}'_2 \in \mathcal{K}\}} \cdot w, \quad w_{(3)} = w.$$

4. Frozen particles are denoted by the collection $\mathcal{S} = \{(\mathbf{x}_i, \mathbf{k}_i)\}_{i=1}^N$ and are weighted by $\mathcal{W} = \{w_i\}_{i=1}^N$, with $w_i \in [-1, 1]$. Any quantum observables \hat{A} can be estimated through Eq. (2.23).
 5. The $(2m - 1)$ -th and $(2m)$ -th particles are suggested to be produced in pair to maintain the mass conservation, say, $\sum_{i=1}^N w_i = N_\alpha$. The particles with weight $w = 0$ are actually not counted in the branching particle system.
-

and the multiplicative functionals ξ/γ in Alg. 1 are chosen to be either $\xi(\mathbf{x}(\tau))/\gamma(\mathbf{x}(\tau)) = 1$ or $-\xi(\mathbf{x}(\tau))/\gamma(\mathbf{x}(\tau)) = -1$, resulting in the signed weights.

The main difficulty lies in the generation of a random life-length τ for each particle. Recall that the lifetime of each particle, initially at time t_0 , satisfies

$$\tau \propto \left. \frac{d\mathcal{G}(t'; \mathbf{x}, t_0)}{dt'} \right|_{t'=t_0+\tau}. \quad (3.2)$$

To draw samples from such a distribution, we can draw a uniform random number u in $[0, 1)$ such that

$$u = \mathcal{G}(t_0 + \tau; \mathbf{x}, t_0), \quad (3.3)$$

and then a simple calculation yields

$$-\ln(1 - u) = \int_{t_0}^{t_0+\tau} \gamma(\mathbf{x}(s - t_0)) ds. \quad (3.4)$$

However, solving Eq. (3.4) for τ is entirely not trivial as the explicit form of $\gamma(\mathbf{x})$ is unknown. As a practical way, we always resort to another approach, starting from a simple fact:

$$\begin{aligned} \frac{d\mathcal{G}(t'; \mathbf{x}, t_0)}{dt'} &= \gamma(\mathbf{x}) e^{-\gamma(\mathbf{x})(t'-t_0)} \cdot \frac{\gamma(\mathbf{x}(t' - t_0)) e^{-\int_{t_0}^{t'} \gamma(\mathbf{x}(s-t_0)) ds}}{\gamma(\mathbf{x}) e^{-\gamma(\mathbf{x})(t'-t_0)}} \\ &= \frac{d\tilde{\mathcal{G}}(t'; \mathbf{x}, t_0)}{dt'} \cdot \eta(\mathbf{x}, t' - t_0), \end{aligned} \quad (3.5)$$

where

$$\frac{d\tilde{\mathcal{G}}(t'; \mathbf{x}, t_0)}{dt'} = \gamma(\mathbf{x}) e^{-\gamma(\mathbf{x})(t'-t_0)}, \quad \eta(\mathbf{x}, \tau) = \frac{\gamma(\mathbf{x}(\tau))}{\gamma(\mathbf{x})} \cdot e^{-\int_{t_0}^{t_0+\tau} [\gamma(\mathbf{x}(s-t_0)) - \gamma(\mathbf{x})] ds}.$$

Therefore, it suffices to take $\tilde{\mathcal{G}}(t'; \mathbf{x}, t_0)$ as the instrumental exponential distribution, yielding

$$\tau \propto \left. \frac{d\tilde{\mathcal{G}}(t'; \mathbf{x}, t_0)}{dt'} \right|_{t'=t_0+\tau}, \quad (3.6)$$

and then the life-length τ reads

$$-\ln(1 - u) = \int_{t_0}^{t_0+\tau} \gamma(\mathbf{x}) ds = \gamma(\mathbf{x}) \tau \Rightarrow \tau = -\frac{\ln(1 - u)}{\gamma(\mathbf{x})}. \quad (3.7)$$

Correspondingly, the factor $\eta(\mathbf{x}, \tau)$ is treated as the importance weight.

sp0 ignores the bias introduced by $\eta(\mathbf{x}, \tau)$, and puts a severe limitation on the time step Δt , as $\eta(\mathbf{x}, \tau) \approx 1$ is only valid when $\tau \leq \Delta t \ll 1$ [12]. By contrast, **wp** attaches $\eta(\mathbf{x}, \tau)$ to the multiplicative functional $\xi(\mathbf{x}(\tau))/\gamma(\mathbf{x}(\tau))$. A careful benchmark in [5] has shown that a longer time step is allowed, while the accuracy is still maintained. A key observation here is that a constant auxiliary function $\gamma(\mathbf{x}) \equiv \gamma_0$ directly leads to $\eta(\mathbf{x}, \tau) \equiv 1$, thereby getting rid of the bias.

The importance of the flexibility on the choice of $\gamma(\mathbf{x}) \equiv \gamma_0$ cannot be exaggerated. First, **wp** allows a variance reduction by enlarging γ_0 , while **sp0** fails to hold such property (*vide post*). Second, the normalizing factor used in Eq. (3.1) becomes very difficult to evaluate when the potential $V(\mathbf{x})$ is a multivariate function [22] (for instance, when it's composed of many components). On the contrary, such difficulty is easily overcome by a constant auxiliary $\gamma(\mathbf{x}) \equiv \gamma_0$ that satisfies

$$\gamma_0 \geq \check{\xi} := \max_m \sup_{\mathbf{x}} \xi_m(\mathbf{x}). \quad (3.8)$$

In this way, the life-length τ of each particle turns out to be

$$\tau = -\frac{\ln(1-u)}{\gamma_0}. \quad (3.9)$$

Third, it's easy to verify the growth rate of particle number satisfies the formula $\mathbb{E}Z_T = e^{2M\gamma_0 T}$ for $\gamma(\mathbf{x}) \equiv \gamma_0$ [5], which helps estimate the memory requirement.

3.2 A probabilistic interpretation of ξ/γ

The first strategy **sp1** interprets ξ/γ as the probability to generate particles. In particular, for $\gamma(\mathbf{x}) \equiv \gamma_0$ satisfying Eq. (3.8), we can easily give an estimation of the growth rate of total particle number for **sp1**.

Theorem 1. *Denote $\mathbb{E}Z_T$ by the expectation of the total number of frozen particles in time interval $[0, T]$. For **sp1**, we have*

$$\mathbb{E}Z_T \leq e^{2M\check{\xi}T}. \quad (3.10)$$

Thus the bound for the averaging particle number is independent of the choice of γ_0 .

Proof. Each particle is produced with probability no more than $\check{\xi}/\gamma_0$ except the last particle, which is produced with probability 1. Thus the expectation $\mathbb{E}Z_t$ satisfies the following inequality

$$\mathbb{E}Z_t \leq 1 - G(t) + \left(\frac{2M\check{\xi}}{\gamma_0} + 1\right) \int_0^t \mathbb{E}Z_{t-u} dG(u), \quad (3.11)$$

with $G(u) = 1 - e^{-\gamma_0 u}$. By the Gronwall's inequality, we have

$$\mathbb{E}Z_t \leq e^{2M\check{\xi}t}. \quad (3.12)$$

By replacing t with T , we have completed the proof. \square

Remark 1. Based on the principle of the rejection resampling, the multiplicative functional ξ/γ can be interpreted by a different approach as given in [13]. It suggests

to seek a positive semidefinite majorant $\hat{V}_w(\mathbf{x}, \mathbf{k})$ such that $|V_w(\mathbf{x}, \mathbf{k})| \leq \hat{V}_w(\mathbf{x}, \mathbf{k})$, then the convolution is rewritten as

$$\begin{aligned} & \int_{\mathcal{K}} d\mathbf{k}' V_w(\mathbf{x}, \mathbf{k} - \mathbf{k}') f(\mathbf{x}, \mathbf{k}', t) \\ &= \gamma(\mathbf{x}) \int_{\mathcal{K}} d\mathbf{k}' \frac{\xi(\mathbf{x})}{\gamma(\mathbf{x})} \cdot \frac{V_w(\mathbf{x}, \mathbf{k} - \mathbf{k}')}{|V_w(\mathbf{x}, \mathbf{k} - \mathbf{k}')|} \cdot \frac{|V_w(\mathbf{x}, \mathbf{k} - \mathbf{k}')|}{\hat{V}_w(\mathbf{x}, \mathbf{k} - \mathbf{k}')} \cdot \frac{\hat{V}_w(\mathbf{x}, \mathbf{k} - \mathbf{k}')}{\xi(\mathbf{x})} f(\mathbf{x}, \mathbf{k}', t). \end{aligned} \quad (3.13)$$

Here $\xi(\mathbf{x})$ is the normalizing factor of the majorant $\hat{V}_w(\mathbf{x}, \mathbf{k})$, instead of $V_w^+(\mathbf{x}, \mathbf{k})$, and it suffices to set $\gamma(\mathbf{x}) = \xi(\mathbf{x})/2$,

$$\gamma(\mathbf{x}) = \frac{1}{2}\xi(\mathbf{x}) = \frac{1}{2} \int_{2\mathcal{K}} \hat{V}_w(\mathbf{x}, \mathbf{k}) d\mathbf{k}. \quad (3.14)$$

Hence each term has a clear probabilistic interpretation. $\hat{V}_w(\mathbf{x}, \mathbf{k} - \mathbf{k}')/\xi(\mathbf{x})$ is the instrumental probability density, $|V_w(\mathbf{x}, \mathbf{k} - \mathbf{k}')|/\hat{V}_w(\mathbf{x}, \mathbf{k} - \mathbf{k}')$ is the probability to generate particles, and $V_w(\mathbf{x}, \mathbf{k} - \mathbf{k}')/|V_w(\mathbf{x}, \mathbf{k} - \mathbf{k}')|$ determines the particle sign. And, the multiplicative functional $\xi(\mathbf{x})/\gamma(\mathbf{x}) = 2$ is regarded as generating two particles carrying opposite signs, according to the fact that

$$\frac{2V_w(\mathbf{x}, \mathbf{k} - \mathbf{k}')}{|V_w(\mathbf{x}, \mathbf{k} - \mathbf{k}')|} = \frac{V_w(\mathbf{x}, \mathbf{k} - \mathbf{k}')}{|V_w(\mathbf{x}, \mathbf{k} - \mathbf{k}')|} - \frac{V_w(\mathbf{x}, \mathbf{k}' - \mathbf{k})}{|V_w(\mathbf{x}, \mathbf{k}' - \mathbf{k})|}. \quad (3.15)$$

Unlike WBRW, this approach avoids the use of an exponential distribution in Eq. (2.1), therefore the life-length τ is not randomly generated. Instead, τ is set to be a fixed value and $\gamma(\mathbf{x})\tau$ is treated to be the probability for generating new offsprings. However, it still requires τ sufficiently small to ensure $\gamma(\mathbf{x})\tau \leq 1$, that hampers the efficiency as a result.

3.3 A bootstrap filter for weighted particles

From the view of computation, **sp1** is advantageous over **wp** in data storage as the sign functions can be operated as integers. However, later we will show that the variance of **sp1** is usually larger than that of **wp** and the accuracy cannot be improved by adjusting γ_0 . The second strategy **sp2** is to get the advantages in both data storage and variance reduction. Based on **wp**, we introduce a bootstrap filtering step to adjust N weighted particles into N signed particles.

The key idea of the bootstrap filtering is to eliminate the particles having low importance weights and to multiply particles having higher importance weights, thereby avoiding the skewness of the particle weights [19, 20, 23]. Mathematically speaking, the target of the bootstrap resampling is to approximate a weighted empirical measure by a unweighted one. In this work, we only utilize the simplest version of bootstrapping for a prototype testing. In fact, more sophisticated bootstrapping techniques, such as the particle island model, may be adopted and one can refer to [24] for more details.

Now suppose we have a collection of N particles, $\mathcal{S} = \{(\mathbf{x}_i, \mathbf{k}_i)\}_{i=1}^N$, which are weighted by the collection $\mathcal{W} = \{w_i\}_{i=1}^N$, $\sum_{i=1}^N w_i = N$. First, we consider $w_i > 0$ and Alg. 2 is just a typical way to achieve the filtering [19], with Lemma 1 giving its variance estimation.

Algorithm 2 Residual bootstrap filtering

1. Retain $k_i = [w_i]$ copies of $(\mathbf{x}_i, \mathbf{k}_i) \in \mathcal{S}$, $i = 1, \dots, N$, where $[w_i]$ indicates the largest integer that doesn't exceed w_i . Let $N_r = N - k_1 - \dots - k_N$.
 2. Obtain N_r i.i.d. draws from \mathcal{S} with probabilities proportional to $w_i - k_i$, $i = 1, \dots, N$.
 3. Assign the weight of 1 to new sample set, denoted by $\tilde{\mathcal{S}} = \{(\tilde{\mathbf{x}}_i, \tilde{\mathbf{k}}_i)\}_{i=1}^N$.
-

Lemma 1. *For any bounded measurable function φ , we have*

$$\mathbb{E} \left| \langle \varphi, \frac{1}{N} \sum_{i=1}^N w_i \delta_{\mathbf{x}_i, \mathbf{k}_i} \rangle - \langle \varphi, \frac{1}{N} \sum_{i=1}^N \delta_{\tilde{\mathbf{x}}_i, \tilde{\mathbf{k}}_i} \rangle \right|^2 \leq 2 \left(\frac{N_r}{N} + 1 \right) \cdot \frac{\|\varphi\|^2}{N}, \quad (3.16)$$

where $w_i > 0$, $\sum_{i=1}^N w_i = N$, $\|\varphi\| = \max |\varphi(x)|$ and the set $\{\tilde{\mathbf{x}}_i, \tilde{\mathbf{k}}_i\}_{i=1}^N$ is produced by Alg. 2.

Now we turn to extend the bootstrap filter to the signed weighted empirical measure, where $w_i \in [-1, 1]$. A natural way is to split the signed particles into two batches according to their signs and thus the signed weighted empirical measure can be decomposed into two weighted ones. Afterwards, we use bootstrap filters to tackle such two empirical measures through Alg. 2 separately.

Suppose we have a collection of N particles, $\mathcal{S} = \{(\mathbf{x}_i, \mathbf{k}_i)\}_{i=1}^N$, which are weighted by the collection $\mathcal{W} = \{w_i\}_{i=1}^N$, with $w_i \in [-1, 1]$ and $\sum_{i=1}^N w_i = N_\alpha$. As discussed above, we can also divide \mathcal{S} into N^+ positive weighted particles $\mathcal{S}^+ = \{(\mathbf{x}_i^+, \mathbf{k}_i^+)\}_{i=1}^{N^+}$ and N^- negative weighted ones $\mathcal{S}^- = \{(\mathbf{x}_i^-, \mathbf{k}_i^-)\}_{i=1}^{N^-}$. Then we can rewrite the signed weighted empirical measure as

$$\begin{aligned} \frac{1}{N_\alpha} \sum_{i=1}^N w_i \delta_{\mathbf{x}_i, \mathbf{k}_i} &= \frac{1}{N_\alpha} \sum_{i=1}^{N^+} w_i^+ \delta_{\mathbf{x}_i^+, \mathbf{k}_i^+} + \frac{1}{N_\alpha} \sum_{i=1}^{N^-} w_i^- \delta_{\mathbf{x}_i^-, \mathbf{k}_i^-} \\ &= \lambda^+ \sum_{i=1}^{N^+} \frac{w_i^+}{\sum_{i=1}^{N^+} w_i^+} \delta_{\mathbf{x}_i^+, \mathbf{k}_i^+} + \lambda^- \sum_{i=1}^{N^-} \frac{w_i^-}{\sum_{i=1}^{N^-} w_i^-} \delta_{\mathbf{x}_i^-, \mathbf{k}_i^-} \\ &= \lambda^+ \sum_{i=1}^{N^+} \tilde{w}_i^+ \delta_{\mathbf{x}_i^+, \mathbf{k}_i^+} + \lambda^- \sum_{i=1}^{N^-} \tilde{w}_i^- \delta_{\mathbf{x}_i^-, \mathbf{k}_i^-}, \end{aligned} \quad (3.17)$$

where

$$\lambda^\pm = \frac{1}{N_\alpha} \sum_{i=1}^{N^\pm} w_i^\pm, \quad \lambda^+ > 0, \quad \lambda^- < 0, \quad (3.18)$$

and \tilde{w}_i^+ and \tilde{w}_i^- are normalized weights for \mathcal{S}^+ and \mathcal{S}^- , respectively.

It remains to employ the bootstrap filter to convert the weighted empirical measures into unweighted ones, yielding the following approximation

$$\frac{1}{N_\alpha} \sum_{i=1}^N w_i \delta_{\mathbf{x}_i, \mathbf{k}_i} \sim \frac{\lambda^+}{N^+} \sum_{i=1}^{N^+} \delta_{\tilde{\mathbf{x}}_i^+, \tilde{\mathbf{k}}_i^+} + \frac{\lambda^-}{N^-} \sum_{i=1}^{N^-} \delta_{\tilde{\mathbf{x}}_i^-, \tilde{\mathbf{k}}_i^-}, \quad (3.19)$$

Similarly, we can derive the variance estimation for such bootstrap filter.

Theorem 2. *For any bounded measurable function φ , we have*

$$\mathbb{E} \left| \left\langle \varphi, \frac{1}{N_\alpha} \sum_{i=1}^N w_i \delta_{\mathbf{x}_i, \mathbf{k}_i} \right\rangle - \left\langle \varphi, \frac{\lambda^+}{N^+} \sum_{i=1}^{N^+} \delta_{\tilde{\mathbf{x}}_i^+, \tilde{\mathbf{k}}_i^+} + \frac{\lambda^-}{N^-} \sum_{i=1}^{N^-} \delta_{\tilde{\mathbf{x}}_i^-, \tilde{\mathbf{k}}_i^-} \right\rangle \right|^2 \leq 8 \left(\frac{|\lambda^+|^2}{N^+} + \frac{|\lambda^-|^2}{N^-} \right) \|\varphi\|^2, \quad (3.20)$$

where $w_i \in [-1, 1]$, $\sum_{i=1}^N w_i = N_\alpha = N^+ - N^-$, $\|\varphi\| = \max |\varphi(x)|$ and the sets $\{\tilde{\mathbf{x}}_i^\pm, \tilde{\mathbf{k}}_i^\pm\}_{i=1}^{N^\pm}$ are produced by Alg. 2.

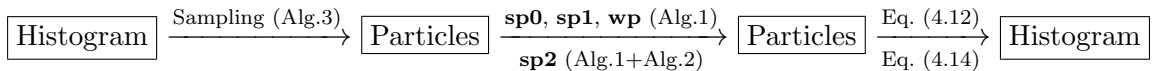
Proof. By the triangle inequality, we have

$$\begin{aligned} & \mathbb{E} \left| \left\langle \varphi, \frac{1}{N_\alpha} \sum_{i=1}^N w_i \delta_{\mathbf{x}_i, \mathbf{k}_i} \right\rangle - \left\langle \varphi, \frac{\lambda^+}{N^+} \sum_{i=1}^{N^+} \delta_{\tilde{\mathbf{x}}_i^+, \tilde{\mathbf{k}}_i^+} + \frac{\lambda^-}{N^-} \sum_{i=1}^{N^-} \delta_{\tilde{\mathbf{x}}_i^-, \tilde{\mathbf{k}}_i^-} \right\rangle \right|^2 \\ & \leq 2 \left| \frac{\sum_{i=1}^{N^+} w_i^+}{N_\alpha} \right|^2 \cdot \mathbb{E} \left| \left\langle \varphi, \frac{1}{N^+} \sum_{i=1}^{N^+} (N^+ \tilde{w}_i^+) \cdot \delta_{\tilde{\mathbf{x}}_i^+, \tilde{\mathbf{k}}_i^+} \right\rangle - \left\langle \varphi, \frac{1}{N^+} \sum_{i=1}^{N^+} \delta_{\tilde{\mathbf{x}}_i^+, \tilde{\mathbf{k}}_i^+} \right\rangle \right|^2 \\ & \quad + 2 \left| \frac{\sum_{i=1}^{N^-} w_i^-}{N_\alpha} \right|^2 \cdot \mathbb{E} \left| \left\langle \varphi, \frac{1}{N^-} \sum_{i=1}^{N^-} (N^- \tilde{w}_i^-) \cdot \delta_{\tilde{\mathbf{x}}_i^-, \tilde{\mathbf{k}}_i^-} \right\rangle - \left\langle \varphi, \frac{1}{N^-} \sum_{i=1}^{N^-} \delta_{\tilde{\mathbf{x}}_i^-, \tilde{\mathbf{k}}_i^-} \right\rangle \right|^2 \\ & \leq |\lambda^+|^2 \cdot \frac{8\|\varphi\|^2}{N^+} + |\lambda^-|^2 \cdot \frac{8\|\varphi\|^2}{N^-}, \end{aligned}$$

where the second inequality utilizes Lemma 1. □

4 Implementation details

A complete period of the WBRW is constituted of three parts: sampling from the Wigner function, running the branching random walk and resampling, in which drawing samples is the crucial step. All the details on the implementation are provided in this section, as sketched by the diagram below.



The histogram provides a compact representation of the particle system and stores all the information in a single matrix. The number of signed particles in each bin and their coordinates are recovered through Alg. 3. Then we simulate their branching

random walks according to Alg. 1 and finally construct a new histogram through Eq. (4.12) for **sp0**, **sp1**, **wp** or Eq. (4.14) for **sp2**.

The WBRW algorithm can be performed in a simple parallelizing manner. For each processor, we pick up several bins and draw one cluster of particles, then run the branching random walk and reconstruct the histogram independently. The remaining task is to merge the histograms. The signed-particle implementations are certainly advantageous because both the updating of particle weights and the merging of histograms, that involves a summation of large matrices, can be performed by integer arithmetic operation.

4.1 Sampling from the Wigner function

Suppose $\{D_j\}_{j=1}^{N_h}$ gives a partition of D , say, D_j are mutually disjoint bins and $D = \bigcup_{j=1}^{N_h} D_j$. The Wigner function at instant t_l is a piecewise constant function (histogram), produced either by the particle reduction in the previous step or by the following construction for the initial data:

$$f(\mathbf{x}, \mathbf{k}, t_l) \approx \sum_{j=1}^{N_h} d_j(t_l) \cdot \mathbb{1}_{D_j}(\mathbf{x}, \mathbf{k}), \quad d_j(t_l) = f(\mathbf{x}_j, \mathbf{k}_j, t_l), \quad (4.1)$$

where N_h is the partition size of the histogram, $(\mathbf{x}_j, \mathbf{k}_j)$ is the centre of the bin D_j and the instrumental distribution is simply given by

$$f_I(\mathbf{x}, \mathbf{k}, t_l) = H(t_l)^{-1} \sum_{j=1}^{N_h} |d_j(t_l)| \cdot \mathbb{1}_{D_j}(\mathbf{x}, \mathbf{k}), \quad H(t_l) = \sum_{j=1}^{N_h} |d_j(t_l)|. \quad (4.2)$$

Now for a given particle size N_α , the initial weighted particles at t_l are sampled through the Alg. 3. The number of particles allocated in D_j is determined by the following rounding step and the initial weight is determined by $|d_j(t_l)|/d_j(t_l)$ according to Eq. (4.2). The coordinate of each particle is produced randomly according to a local uniform distribution.

Remark 2. It notes that for **sp1**, the importance sampling is greatly simplified as m is an integer according to Eq. (4.13). Therefore, the rounding step in Alg. 3 can be skipped.

4.2 Run the Wigner Branching Random Walk

After allocating the particles at the instant t_l , we begin to simulate the branching random walk of particles until t_{l+1} according to Alg. 1. We require to draw samples according to the splitted Wigner kernel and calculate $\xi(\mathbf{x})$, both of which can be resolved by a simple rejection method.

The key of rejection sampling is to find an appropriate sampling distribution and a covering constant [23]. Suppose we would like to draw samples according to

Algorithm 3 Importance sampling from the quasi-probability density

1. (Rounding step) Draw a random number u from the uniform distribution in $[0, 1)$ and determine the particle number n_j in D_j by

$$n_j = [m] + p, \quad m = N_\alpha \cdot \mu(D_j) \cdot |d_j(t_l)|, \quad (4.3)$$

where $[m]$ is the integer part of m and

$$p = \begin{cases} 1, & u \leq m - [m], \\ 0, & u > m - [m]. \end{cases} \quad (4.4)$$

2. Endow each particle in the bin D_j with a weight $|d_j(t_l)|/d_j(t_l) = \pm 1$.
 3. Endow each particle in the bin D_j with a random coordinate (\mathbf{x}, \mathbf{k}) according to the local uniform distribution $(\mu(D_j))^{-1} \cdot \mathbb{1}_{D_j}(\mathbf{x}, \mathbf{k})$.
-

$V_w^+(\mathbf{x}, \mathbf{k})/\xi(\mathbf{x})$. For a fixed \mathbf{x} , it's necessary to find a normalized sampling distribution $g(\mathbf{k})$ and a covering constant M , such that

$$V_w^+(\mathbf{x}, \mathbf{k}) \leq Mg(\mathbf{k}). \quad (4.5)$$

The rejection sampling can also be used in calculating the normalizing factor $\xi(\mathbf{x})$. In order to reduce the computational cost, we can calculate $\xi(\mathbf{x})$ on a grid mesh in advance, and use interpolations to obtain the points that are not located on the mesh. Actually, linear interpolation is a desirable choice to strike a balance between accuracy and efficiency, as $\xi(\mathbf{x})$ is very flat except a small central region, where it decays to 0 sharply.

Algorithm 4 Rejection sampling from $V_w^+(\mathbf{x}, \cdot)$

1. Draw a sample \mathbf{k} from $g(\mathbf{k})$ and compute the ratio $p = V_w^+(\mathbf{x}, \mathbf{k})/[Mg(\mathbf{k})]$.
 2. Draw a uniform random number u in $[0, 1)$.
 3. If $p < u$, we accept and return \mathbf{k} ; otherwise, we reject \mathbf{k} and go back to step 1.
-

We mainly focus on the potential with symmetry along an axis $\mathbf{x} = \mathbf{x}_c$

$$V(\mathbf{x}_c + \mathbf{x}) = V(\mathbf{x}_c - \mathbf{x}), \quad (4.6)$$

such as the Gaussian barrier and two-body Yukawa interactions, and the corresponding Wigner kernel reads

$$V_w(\mathbf{x}, \mathbf{k}) = \frac{2}{\hbar} \cdot \hat{V}(2\mathbf{k}) \sin(2(\mathbf{x} - \mathbf{x}_c) \cdot \mathbf{k}), \quad (4.7)$$

where \hat{V} denotes the Fourier transform of V . In the experiments, we will use the following relations:

$$V(x) = \frac{1}{\sqrt{2\pi}} e^{-x^2/2}, \quad \hat{V}(k) = \sqrt{\frac{2}{\pi}} e^{-2k^2}, \quad (4.8)$$

$$V(x) = \frac{e^{-\kappa|x|}}{2\kappa}, \quad \hat{V}(k) = \frac{1}{k^2 + \kappa^2}. \quad (4.9)$$

Subsequently, it suffices to choose the majorant $g(k) = \hat{V}(2k)$ and the covering constant $M = 1/\hbar$. The ratio p reduces to $[\sin(2(\mathbf{x} - \mathbf{x}_c) \cdot \mathbf{k})]^+$, where $[\cdot]^+$ means the positive part. When \hat{V} does not have a close form, drawing according to $g(\mathbf{k})$ becomes a tough task and one has to resort to the rejection sampling, like Eq. (3.13) or other advanced techniques, such as the Markov Chain Monte Carlo method [23].

According to Alg. 4, the probability of accepting a proposed sample is proportional to p , thus its efficiency will deteriorate when $|\mathbf{x} - \mathbf{x}_c|$ is sufficiently small. A simple trick, without bias, is introduced here to solve this problem. Suppose $\hat{V}(2\mathbf{k})$ is positive semidefinite, since

$$\frac{V_w^+(\mathbf{x}, \mathbf{k})}{\xi(\mathbf{x})} = \frac{2\xi_0[\sin(2(\mathbf{x} - \mathbf{x}_c) \cdot \mathbf{k})]^+}{\hbar\xi(\mathbf{x})} \cdot \frac{\hat{V}(2\mathbf{k})}{\xi_0}, \quad \xi_0 = \int_{2\mathcal{K}} \hat{V}(2\mathbf{k}) d\mathbf{k}, \quad (4.10)$$

it suffices to treat $\hat{V}(2\mathbf{k})/\xi_0$ as the instrumental probability density and the remainder as the importance weights. To confine the particle weights in $[-1, 1]$, we further require that

$$\frac{2\xi_0[\sin(2(\mathbf{x} - \mathbf{x}_c) \cdot \mathbf{k})]^+}{\hbar\xi(\mathbf{x})} \leq 1, \quad (4.11)$$

which always holds when $|\mathbf{x} - \mathbf{x}_c|$ is sufficiently small.

4.3 Resampling of particles

The resampling technique intends to control the particle number in the simulations, as well as suppress the growth of variances. It arises from the fact that the branching treatment will inevitably lead to an exponential growth of particle number, which is undesirable for long-time simulations (see Theorem 1).

The terminology ‘resampling’, in fact, has different meanings in different applications. In the diffusion Monte Carlo or the sequential importance sampling, the resampling procedure, also called the bootstrap filtering, is to adjust the skewness of importance weights [20]. In the Boltzmann simulations, the so-called particle resampling is aimed at reducing the number of positive and negative particles, which describe the deviation from the Maxwell distribution [10,11]. As summarized in [11], the particle reduction strategies are roughly divided into three categories: the particle cancellation, the particle thermalization and the spectral filtering. In the Wigner simulations, the particle cancellation is naturally adopted due to the sign weights which reflect both positive and negative values of the Wigner function. It borrows the idea of histogram [17,18] and is essentially a piecewise constant reconstruction

of a (quasi-)density function. The output will be set as the initial data for the next period, from which a new set of particles is drawn through the importance sampling as presented in Alg. 3.

Suppose all particles lie in a compact set $D \subset \mathbb{R}^n$ and $\{D_j\}_{j=1}^{N_h}$ is a partition of D . For \mathbf{wp} , a piecewise constant function $p(\mathbf{x}, \mathbf{k})$ has the form

$$p(\mathbf{x}, \mathbf{k}) = \sum_{j=1}^{N_h} \frac{\sum_{i=1}^N w_i \cdot \mathbb{1}_{D_j}(\mathbf{x}_i, \mathbf{k}_i)}{N_\alpha} \cdot \frac{\mathbb{1}_{D_j}(\mathbf{x}, \mathbf{k})}{\mu(D_j)}. \quad (4.12)$$

In particular, for $\mathbf{sp1}$, since the weight of each particle is either -1 or 1 , we only need to count the particle number in each bin and sum over their signs, yielding

$$p(\mathbf{x}, \mathbf{k}) = \sum_{j=1}^{N_h} \frac{n_i^+ - n_i^-}{N_\alpha} \cdot \frac{\mathbb{1}_{D_j}(\mathbf{x}, \mathbf{k})}{\mu(D_j)}, \quad (4.13)$$

where n_j^+ and n_j^- are counts of the positive and negative particles in D_j , respectively. Since the particles carrying opposite signs are eliminated, such procedure is also called particle cancelation (annihilation) [9, 11].

The construction of the histogram in $\mathbf{sp2}$ is a composition of two histograms, based on filtered positive and negative particles. Starting from Eq. (3.19), we have

$$\tilde{p}(\mathbf{x}, \mathbf{k}) = \sum_{j=1}^{N_h} \left(\frac{\lambda^+ \tilde{n}_j^+}{N^+} + \frac{\lambda^- \tilde{n}_j^-}{N^-} \right) \cdot \frac{\mathbb{1}_{D_j}(\mathbf{x}, \mathbf{k})}{\mu(D_j)}, \quad (4.14)$$

where \tilde{n}_j^+ and \tilde{n}_j^- are counts of the filtered N^+ positive and N^- negative particles in D_j , respectively.

The remaining task is to choose the bins D_j , which are usually (hyper-)rectangles based on a given partition of D . The simplest and most ubiquitous choice is to place a uniform grid mesh $D_j = \mathcal{X}_{j_1} \times \mathcal{K}_{j_2}$, with ϵ denoting the maximal diameter

$$\epsilon = \max_j \sup_{\mathbf{y}_1, \mathbf{y}_2 \in D_j} \|\mathbf{y}_1 - \mathbf{y}_2\|. \quad (4.15)$$

The following theorem presents the error bound $\mathcal{O}(\epsilon)$ for such kind of histogram.

Theorem 3. *Suppose $\{D_j\}_{j=1}^{N_h}$ gives a partition on a compact set $D \subset \mathbb{R}^{2n}$ with the maximal diameter ϵ . Let φ be a bounded measurable function on D and locally Hölder continuous in each bin D_j , say,*

$$\|\varphi\|_{C^{0,\alpha}} = \max_j \sup_{\mathbf{y}_1 \neq \mathbf{y}_2 \in D_j} \frac{|\varphi(\mathbf{y}_1) - \varphi(\mathbf{y}_2)|}{\|\mathbf{y}_1 - \mathbf{y}_2\|^\alpha} < \infty \quad (4.16)$$

for an exponent $\alpha > 0$. Then we have

$$\left| \left\langle \varphi, \frac{1}{N_\alpha} \sum_{i=1}^N w_i \delta_{\mathbf{x}_i, \mathbf{k}_i} \right\rangle - \langle \varphi, p \rangle \right| \leq (|\lambda^+| + |\lambda^-|) \cdot \|\varphi\|_{C^{0,\alpha}} \cdot \epsilon^\alpha, \quad (4.17)$$

where p is given by Eq. (4.12). Moreover, for the piecewise constant reconstruction \tilde{p} in Eq. (4.14), it further yields

$$\mathbb{E}|\langle \varphi, \frac{1}{N_\alpha} \sum_{i=1}^N w_i \delta_{\mathbf{x}_i, \mathbf{k}_i} \rangle - \langle \varphi, \tilde{p} \rangle|^2 \leq C_1 \|\varphi\|_{C^{0,\alpha}}^2 \cdot \epsilon^{2\alpha} + C_2 \frac{\|\varphi\|^2}{N_\alpha}, \quad (4.18)$$

where

$$C_1 = 2(|\lambda^+| + |\lambda^-|)^2, \quad C_2 = 16N_\alpha \left(\frac{|\lambda^+|^2}{N^+} + \frac{|\lambda^-|^2}{N^-} \right).$$

Theorem 3 guarantees the convergence of both the uniform histogram and the bootstrap filtering if letting $\epsilon \rightarrow 0$ and $N_\alpha \rightarrow \infty$. Numerical experiments in the next section will demonstrate that the resampling based on a uniform partition works well when sample size N_α is comparable to N_h , and works poorly when $N_\alpha \ll N_h$ due to the curse of dimensionality as expected [11, 18].

5 Performance evaluation

We have already illustrated both theoretical and numerical aspects of the computable WBRW, and now it resorts to some benchmark tests for a detailed performance evaluation and to show how the choices of parameters influence the accuracy and the efficiency.

Two typical test problems are considered as already employed in [5]: the 2D Gaussian scattering and the 4D Helium-like system. All the parameters are identical to those in [5], except that the averaged position x_0 of the initial data in the 2D problem is reset to be -10 . Under this new initial position can we observe the scattering phenomenon clearly for a relatively short final time $t_{fin} = 10\text{fs}$. Performance metrics include the normalized relative errors for the Wigner function $\text{err}_{wf}(t)$, the spatial marginal density $\text{err}_{sm}(t)$ and the momental marginal density $\text{err}_{mm}(t)$. For details, the readers can refer to [5].

For resampling, we divide equally the time interval $[0, t_{fin}]$ into n_A subintervals with the partition being

$$0 = t^0 < t^1 < t^2 < \dots < t^{n_A} = t_{fin}, \quad n_A = t_{fin}/T_A. \quad (5.1)$$

The resampling occurs at t^i , with $1/T_A$ the resampling frequency. The time step is denoted by Δt . The number of particles after resampling at the instant t is denoted by $\#_P^a(t)$.

5.1 Particle size N_α

We claim that the accuracy can be systematically improved by increasing the particle size N_α . The simulations of the 2D Gaussian scattering are performed with the auxiliary function $\gamma = 1.5\check{\xi}$ and $T_A = 1\text{fs}$ fixed. First, pure Monte Carlo simulations are performed to examine the theoretical convergence order $\mathcal{O}(N_\alpha^{-1/2})$ at $t_{fin} = 10\text{fs}$. Afterwards the resampling is turned on and the experiments are

reinitialized under different sample sizes N_α ranging from 1×10^5 to 10^7 , as presented in Fig. 1 and Fig. 2. Six groups of the 4D Helium-like system are also simulated with N_α ranging from 10^6 to 10^8 , $\gamma = 2$ and $T_A = 0.5\text{a.u.}$ The convergence rate with respect to N_α (at $t_{fin} = 20\text{a.u.}$) is shown in Fig. 3. To visualize the numerical errors, we plot both the spatial and momental marginal distributions under different instants $t = 5, 10, 15, 20\text{a.u.}$ in Fig. 4 and the reduced Wigner function at the instant $t = 20\text{a.u.}$ in Fig. 5. Based on these numerical results, we are able to find out the following observations.

- (1) The accuracy can be systematically improved by increasing the sample size N_α . We find that the convergence order of the pure Monte Carlo method perfectly coincides with the theoretical prediction of $-1/2$, whereas there exists some deviations when the resampling is turned on. Too small N_α yields very poor numerical results, as shown in Figs. 4 and 5. The severe oscillations even shadow the true solution and the reduced Wigner function is too noisy to be observed. As N_α goes larger, the results produced by **sp1** and **wp** fit the spatial marginal density and momentum marginal better, and the stochastic noises in the (reduced) Wigner function are significantly suppressed.
- (2) The stochastic errors grow exponentially in time, so does the variance of the branching random walk model [25]. The accumulation of stochastic errors, in fact, may be related to the time evolution of the quadratic variation of the branching random walk. On the contrary, the resampling, although introducing some deterministic errors as shown in Theorem 3, helps to suppress the random noises significantly.
- (3) Under the same constant auxiliary function γ , **wp** provides more accurate results than **sp1**. However, when N_α is chosen sufficiently large (such as $N_\alpha = 10^7$ in the 2D test and $N_\alpha = 10^8$ in the 4D test), both implementations produce the numerical results with almost the same accuracy. Although the particle number after resampling in **sp1** is larger than that of **wp**, the requirement of memory is even alleviated as the histogram is stored in an integer-valued matrix for the former.

5.2 Variance and the choice of the auxiliary function γ

Another factor that influences the quality of a stochastic estimator is the variance. In this part, we will observe that increasing the auxiliary function γ in **sp1** fails to lead to a systematic improvement on the accuracy, whereas **wp** allows a variance reduction [5]. To study how the choice of a constant auxiliary function γ influences the variance, we perform six groups of the 2D Gaussian scattering with the sample size $N_\alpha = 1 \times 10^7$ and the final time $t_{fin} = 10\text{fs.}$ The resampling is turned off here in order to get rid of the deterministic errors. The results are shown in Figs. 6 and 8(a), from which we can figure out the following lessons.

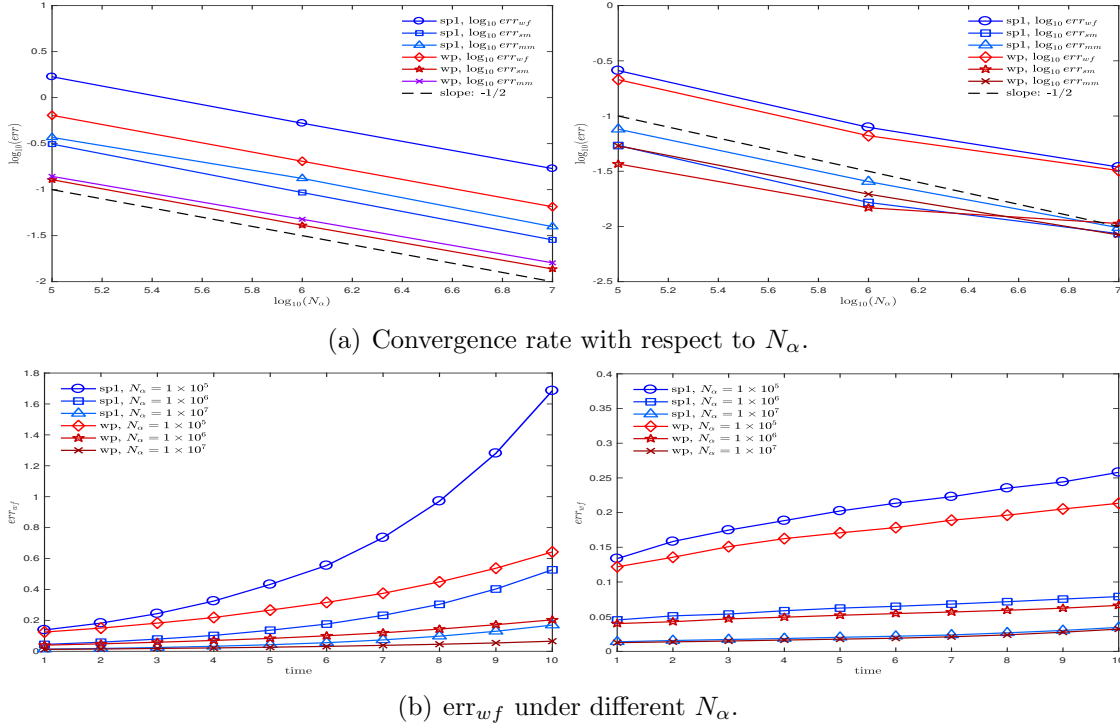
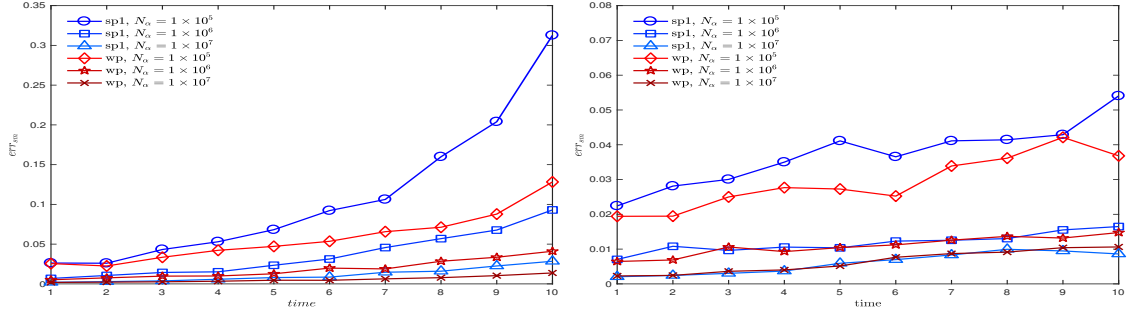


Figure 1: A comparison between pure Monte Carlo simulations (left) and resampling-included simulations (right) for the 2D Gaussian scattering: Convergence rate with respect to N_α and time evolution of relative errors of the Wigner function. For the pure Monte Carlo, the convergence rates of both **sp1** and **wp** accord with the theoretical value $-1/2$. The resampling mechanisms effectively suppress the exponential growth of stochastic noises. Here we set $\gamma = 1.5\tilde{\xi}$ and $T_A = 1\text{fs}$.

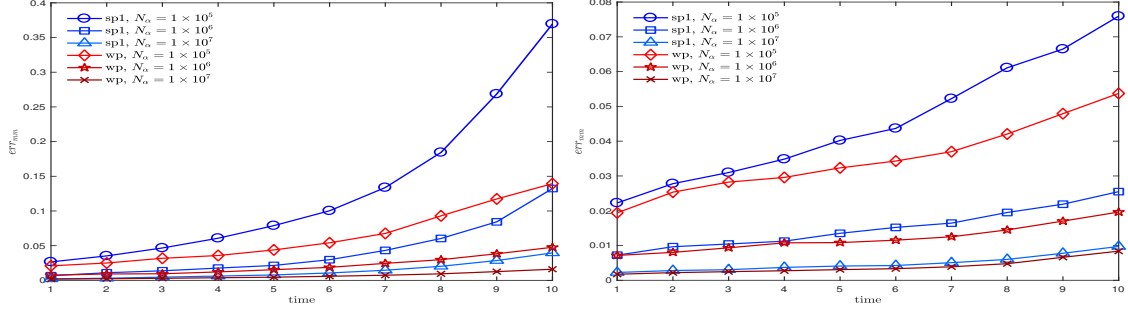
- (1) For **sp1**, the choice of γ has little influence on the accuracy, which may imply that the quadratic variation of **sp1** doesn't depend on the choice of the auxiliary function. By contrast, **wp** clearly allows a variance reduction as the stochastic errors decrease sharply when γ increases. Furthermore, the numerical convergence rate with respect to γ is about $\mathcal{O}(\gamma^{-2})$.
- (2) The growth rate of particle number N/N_α in **sp1** is also independent of γ , as we have predicted in Theorem 1. Actually, the growth rate is slightly smaller than the theoretical upper bound $e^{2\tilde{\xi}t}$, and in **wp** the growth rate is very close to the theoretical prediction of $e^{2\gamma t}$.

5.3 Accuracy and efficiency of resampling

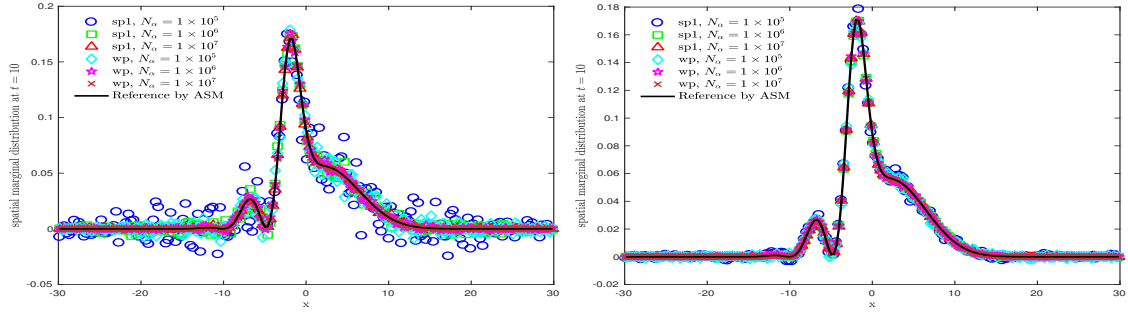
The accuracy of resampling is closely related to the resampling frequency $1/T_A$, while the efficiency depends on the particle size N_α and the partition size N_h . We simulate six groups of the 2D Gaussian scattering with $N_\alpha = 10^7$ and $\gamma = 1.5\tilde{\xi}$, as well as four groups of the 4D Helium-like system with $N_\alpha = 1 \times 10^8$ and $\gamma = 2$. The results under different T_A are compared in Fig. 7. In addition, we collect the data on



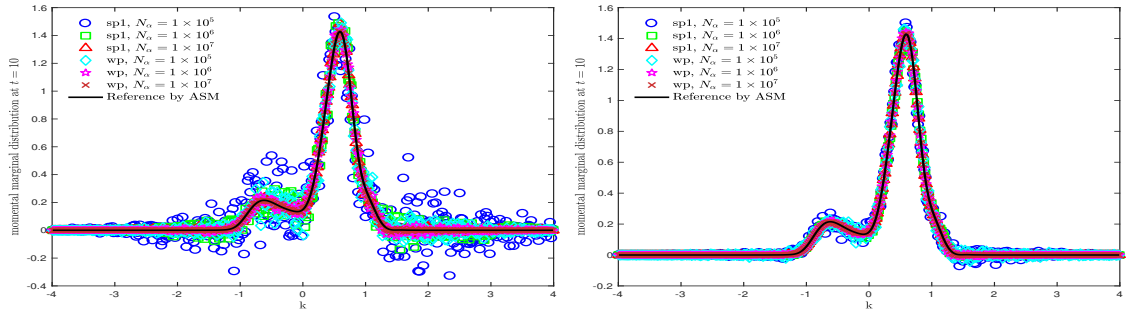
(a) err_{sm} under different N_α .



(b) err_{mm} under different N_α .



(c) Spatial marginal density at $t = 10fs$.



(d) Momental marginal density at $t = 10fs$.

Figure 2: A comparison between pure MC simulations (left) and resampling-included simulations (right) for the 2D Gaussian scattering: Time evolution of relative errors and both spatial and momental marginal distributions at $t = 10fs$ are plotted. Stochastic noises of **sp1** are larger than those of **wp**. Nevertheless, they can be significantly suppressed by increasing N_α . Here we set $\gamma = 1.5\check{\xi}$ and $T_A = 1fs$.

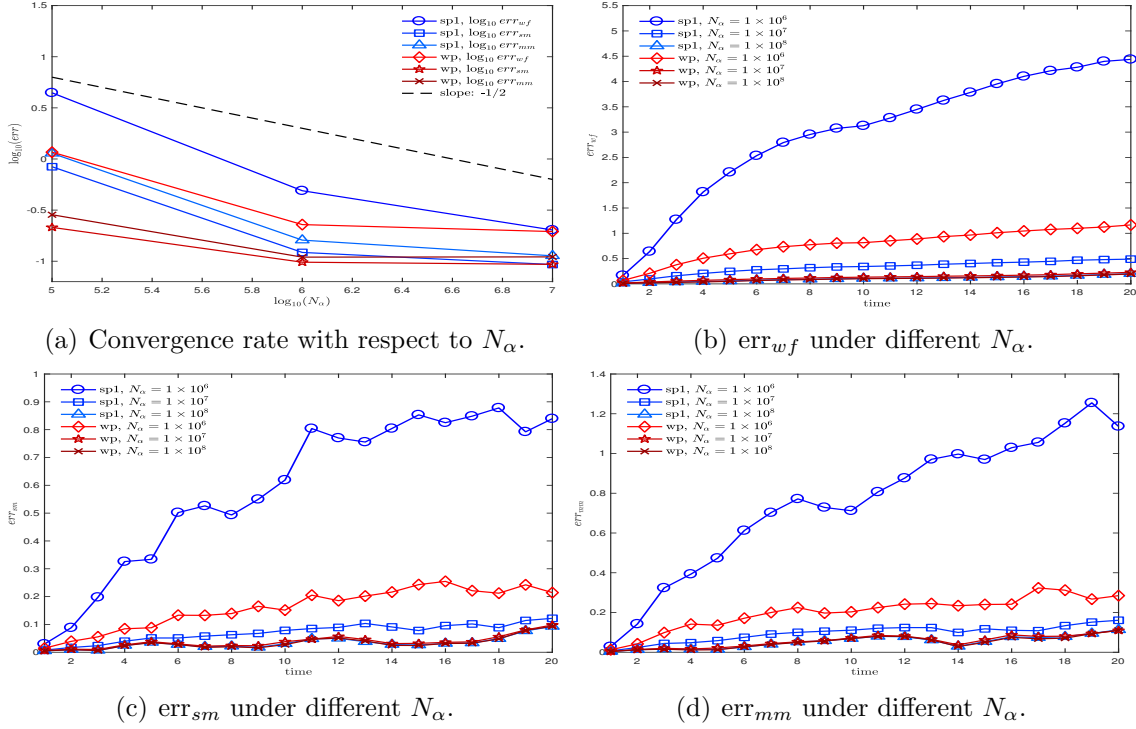


Figure 3: The 4D Helium-like system: Convergence rate and relatives errors under different sample sizes N_α . The convergence rate slightly deviates from the theoretical prediction due to the error of the resampling. Stochastic noises of **sp1** are larger than those of **wp**, but accuracy can be still be improved by increasing N_α . Here we set $\gamma = 2$ and $T_A = 2\text{a.u.}$

the growth rate of particle number N/N_α and the particle number after resampling $\#_P^a$ in the previous simulations. The numerical results uncover the following facts.

- (1) We have evidence that the resampling procedure is indispensable for two reasons. First, the particle number in pure Monte Carlo simulations will inevitably grow exponentially and soon exceeds the limit of memory storage, while the resampling procedure can significantly kill the redundant particles and suppress the particle growth, as shown in Fig. 8(a). Second, although the resampling introduces an additional error term, it suppresses the stochastic errors in the Monte Carlo simulation, thereby improving the accuracy as presented in Fig. 2.
- (2) Too frequent resampling leads to a smaller $\#_P^a$, at the cost of the decline in the accuracy for both 2D and 4D simulations. On the other hand, too low frequency does not necessarily improve the accuracy, as presented in Fig. 7, due to the accumulation of stochastic errors. Therefore, there may be an optimal choice of T_A to strike the balance between the accuracy and the efficiency as already proposed in [5].
- (3) The efficiency of resampling is measured by $\#_P^a$. We can clearly see that the resampling performs quite well when $N_\alpha \geq N_h$. However, according to Fig. 8, it works not so efficiently when $N_\alpha < N_h$. For instance, when $N_h = 10^8$

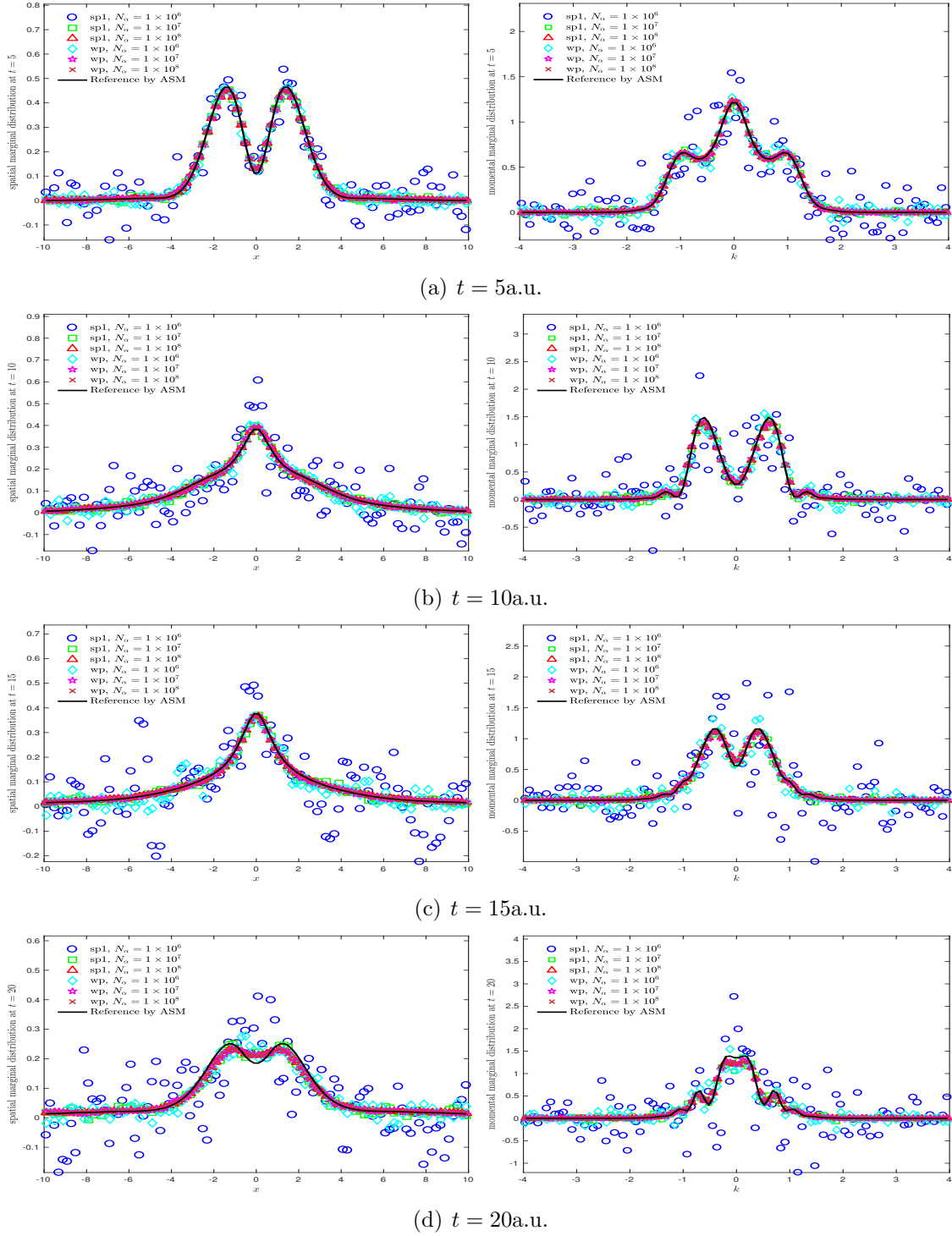


Figure 4: The 4D Helium-like system: Plots of spatial and momental marginal distributions at different instants 5, 10, 15, 20a.u. Too small sample size undermines the accuracy and noises even overshadow the true solutions. For large N_α , both **sp1** and **wp** perform quite well. Here we set $\gamma = 2$ and $T_A = 0.5$ a.u.

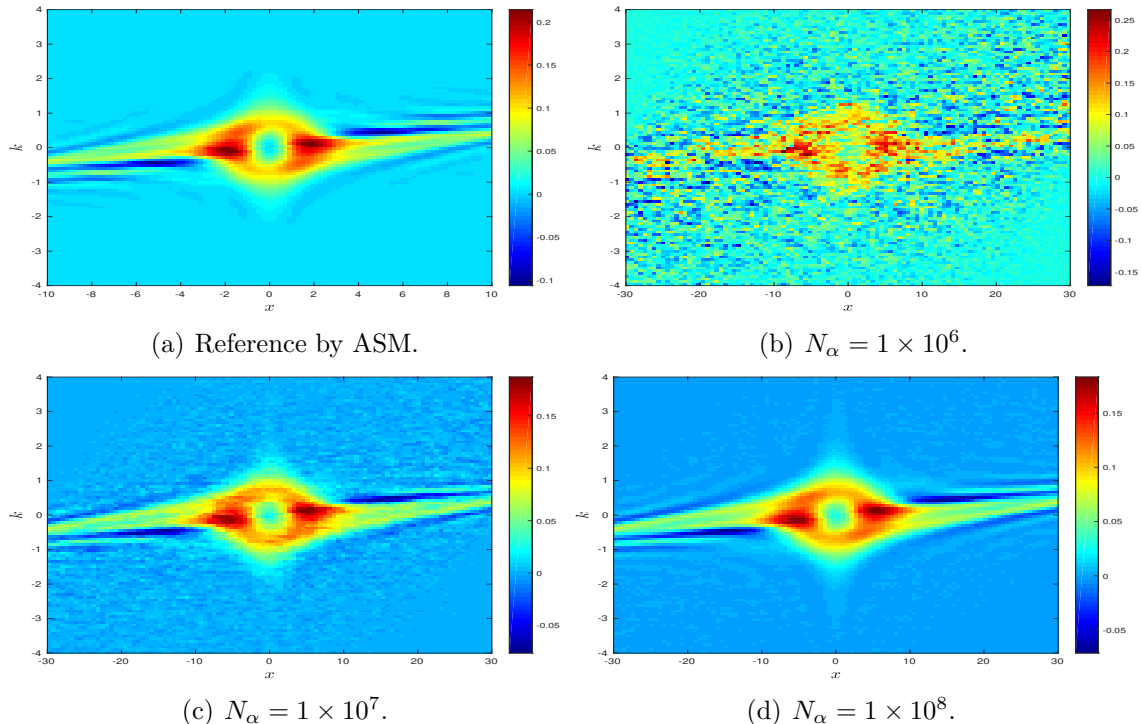


Figure 5: The 4D Helium-like system: Reduced Wigner function at $t_{fin} = 20\text{a.u.}$ under different particle size N_α . The stochastic noises are clearly suppressed by increasing N_α .

and $N_\alpha = 10^6$ in the 4D problem, $\#_P^a$ soon goes to the magnitude of the partition size and finally the particle number exceeds 10^9 , in which the rate $\#_P^a/N_\alpha$ is almost 728 (**sp1**). Even for 2D problem, when $N_\alpha = 1 \times 10^4$ and $N_h = 8 \times 10^4$, we also find that $\#_P^a$ increases dramatically and exceeds 7.7×10^4 at the final stage. Therefore, the ‘‘bottom line’’ structure described in [12] depends on not only the oscillating structure of the Wigner function, but also the partition size N_h . These observations reveal the potential weakness of the uniform histogram, as also pointed out in the statistical community. Actually, to maintain the same accuracy for the high dimensional histogram, the number of samples must also grow exponentially, otherwise a severe ‘overfitting’ will be observed [18]. In practice, $N_\alpha \approx 10N_h$ is a balanced choice in consideration of the efficiency of the resampling. But this condition limits the applicability of the uniform histogram in high dimensional problems.

- (4) $\#_P^a$ is usually larger in **sp1** than that in **wp**, although the converse is true for the growth rate of particle number. In fact, the variance reduction in **wp** helps suppress more random noises and kill more redundant particles. Fortunately, the advantage in storing signed weights saves the performance of **sp1**.
- (5) We record the total running time and the averaged value of $\#_P^a$ (denoted by $\bar{\#}_P^a$) in Table 1, with the computing platform: Intel(R) Xeon(R) CPU E5-2680 v4 (2.40GHz, 35MB Cache, 9.6GT/s QPI Speed, 14 Cores, 28 Threads) and 256GB Memory (we use 14 threads for each task). It is readily seen

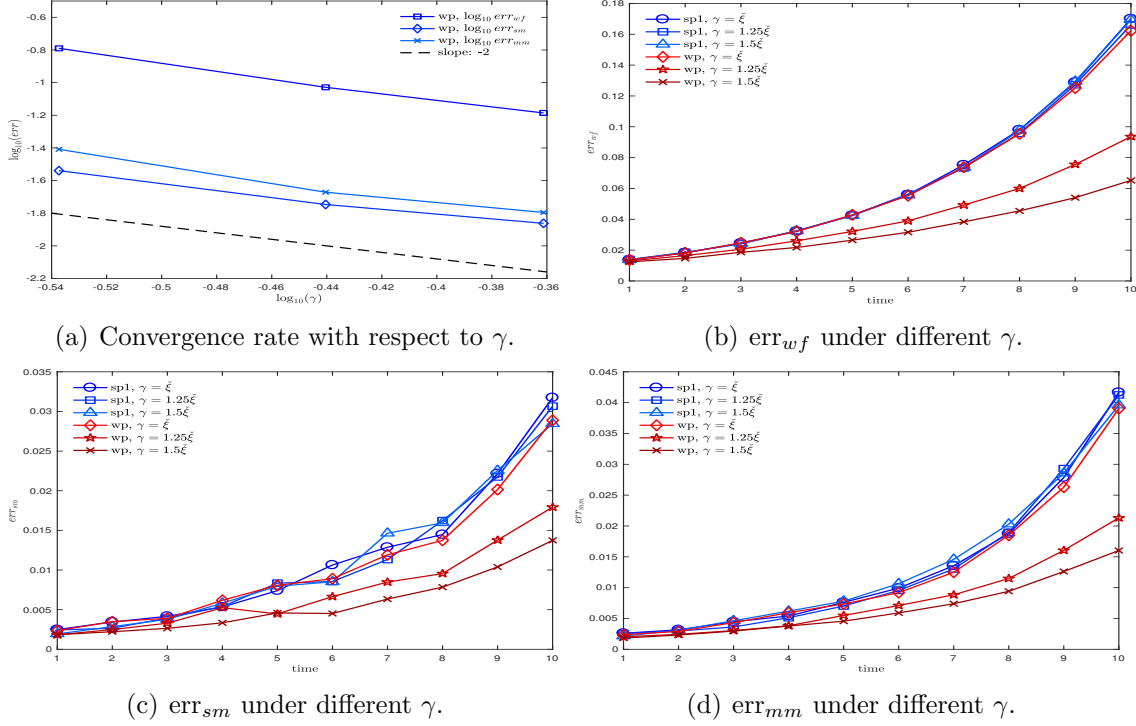


Figure 6: The 2D Gaussian scattering: Relative errors under different constant auxiliary function γ and the convergence rate for at $t_{fin} = 10\text{fs}$. The accuracy of **wp** is improved as γ increases, and the numerical convergence rate is $\mathcal{O}(\gamma^{-2})$. On the contrary, the accuracy of **sp1** cannot be improved by adjusting γ . Here we set the particle size $N_\alpha = 1 \times 10^7$ and the resampling is not used.

there that the computational time is indeed proportional to $\bar{\#}_P^a$, instead of N_α . This means the efficiency of WBRW depends largely on the quality of resampling. Although $\bar{\#}_P^a$ is usually larger, **sp1** is significantly faster because of the moderate growth of particle number.

Table 1: The 4D Helium-like system: $\bar{\#}_P^a$ at $t = 20\text{a.u.}$ and the total running time.

	sp1			wp		
N_α	1×10^6	1×10^7	1×10^8	1×10^6	1×10^7	1×10^8
$\bar{\#}_P^a$	9.03×10^8	9.40×10^8	1.19×10^9	2.42×10^8	2.67×10^8	4.97×10^8
time(h)	44.949	46.837	59.666	51.792	64.033	162.313

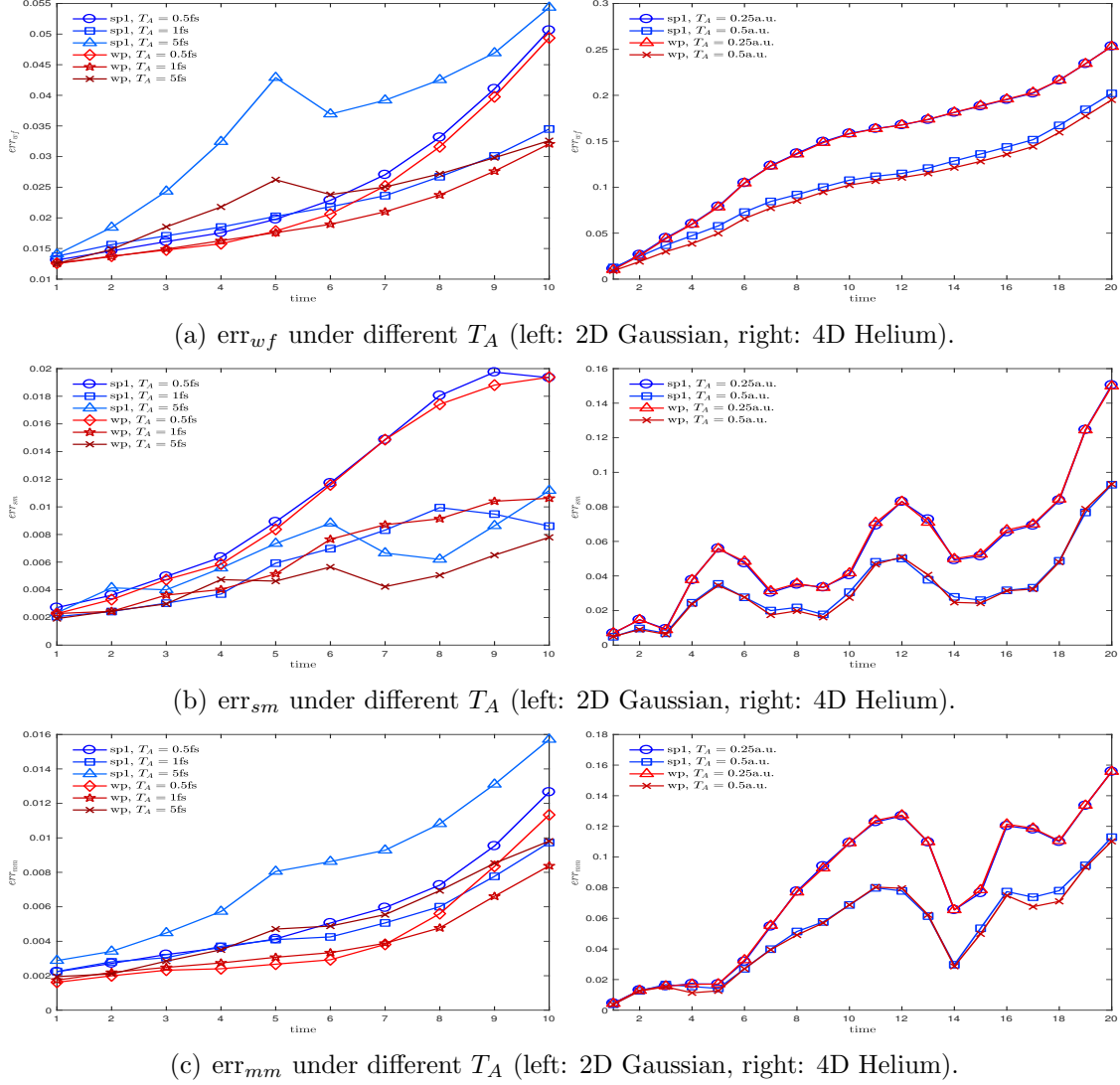
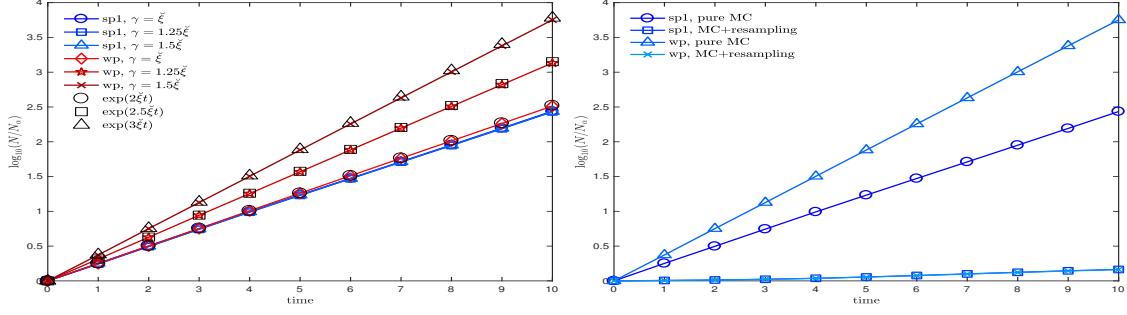


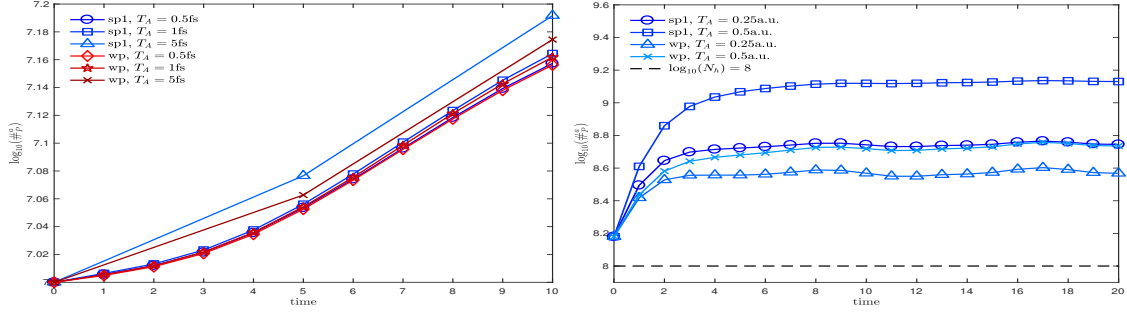
Figure 7: The relative errors of the Wigner function, spatial and marginal distributions for the 2D Gaussian scattering (left) and the 4D Helium-like system (right). The relation between the relative errors and the resampling frequency $1/T_A$ is revealed. Too frequent resampling leads to a decline in the accuracy, while too low frequency also leads to an accumulation of stochastic errors and diminish the accuracy as a result. $\gamma = 1.5\check{\xi}$, $N_\alpha = 1 \times 10^7$, and $\gamma = 2$, $N_\alpha = 1 \times 10^8$ are set for the 2D and 4D simulations, respectively.

5.4 Bootstrap filtering

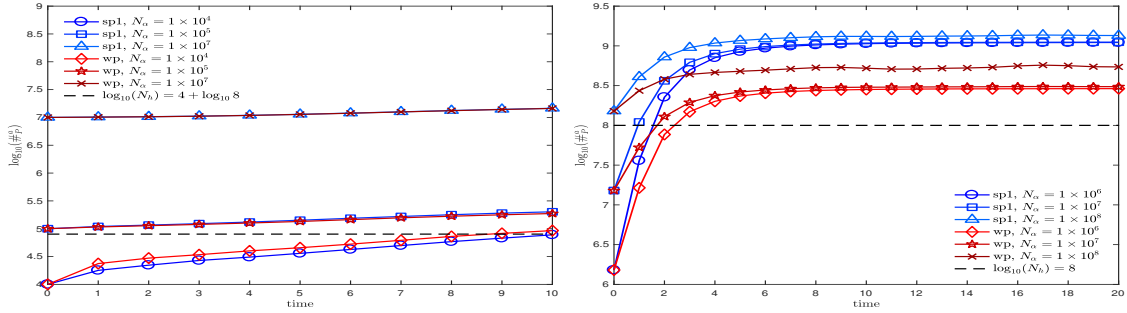
The bootstrap filtering is introduced to adjust the weights to $\{-1, 1\}$, thereby permitting us to store the histogram in two integer-valued matrices (for positive and negative particles). On the other hand, it brings some stochastic noises which diminish as $N_\alpha \rightarrow \infty$. To compare the accuracy of **sp1**, **sp2** and **wp**, we perform four groups of the 2D Gaussian scattering with $\gamma = 3\check{\xi}$ and $T_A = 1$ fs. Three kinds of the particle size $N_\alpha = 10^5, 10^6$ and 10^7 are considered. Then to show the relation between the variance in **sp2** and the auxiliary function γ , we also do four groups



(a) Growth rate of particle number (2D Gaussian).



(b) $\#_P^a$ under different T_A (left: 2D Gaussian, right: 4D Helium).



(c) $\#_P^a$ under different N_α (left: 2D Gaussian, right: 4D Helium).

Figure 8: Relation between the growth of particle number and several factors: γ , particle size N_α , resampling frequency $1/T_A$ and the partition size N_h . The particle number grows exponentially in time and is suppressed by resampling. More frequent resampling leads to a smaller $\#_P^a$. However, the efficiency of resampling deteriorates when N_h is very large, and $\#_P^a$ finally becomes stable in a level that is comparable to N_h .

of simulations with $N_\alpha = 1 \times 10^7$ and $T_A = 1\text{fs}$. Four constant auxiliary functions, ranging from $\check{\xi}$ to $4\check{\xi}$, are adopted. All the numerical results are shown in Fig. 9, from which we can figure out the following observations.

- (1) As the bootstrap filtering introduces some additional random errors, the accuracy of **sp2** lies between those of **sp1** and **wp**. **sp2** also converges as the sample size N_α increases, although the converge rate is slightly deviated from the order $-1/2$.
- (2) **sp2** inherits the advantages in **wp** as increasing γ leads to an evident improvement on the accuracy. Therefore, it successfully seizes the property of variance

reduction of **wp**. However, the convergence of **sp2** with respect to γ is slower than that of **wp** due to the additional stochastic noises.

- (3) **sp2** utilizes two integer-valued matrices, instead of a double-valued one, for storing the histogram. This enables us to establish the histogram by simply counting the particle number in each bin and recording the coefficients λ^\pm defined in Eq. (3.18). The memory requirement of **sp2** is the same as **wp**, and twice more than **sp1**. For example, when $N_h = 100^4$, the memory for storing the histogram is 763MB for **wp** or **sp2**, and 382MB for **sp1**.

The bootstrap filtering indeed achieves the target as we have expected. Although it seems difficult to compare the deterministic errors induced by the histogram approximation and stochastic errors induced by the bootstrap filtering, there may be an optimal choice of γ , N_α and ϵ to achieve a better convergence according to the theoretical error bound (4.18).

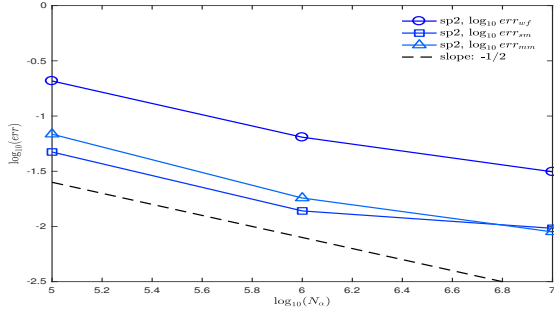
5.5 A comparison between **sp0** and the WBRW

Finally, we would like to make a comparison between our proposed strategies and the existed **sp0**. As we have already demonstrated in Section 3.1, the major advantage of WBRW over **sp0** is that it alleviates the strict restriction on the time step Δt . To clarify it, we simulate the 2D Gaussian scattering with $N_\alpha = 1 \times 10^7$, $T_A = 1\text{fs}$ under five kinds of Δt : 0.01, 0.1, 0.25, 0.5, 1fs. The numerical solutions are compared with those produced by **sp1**, **sp2** and **wp** with $\gamma = \check{\xi}$. Two facts below are observed from the numerical results presented in Fig. 10.

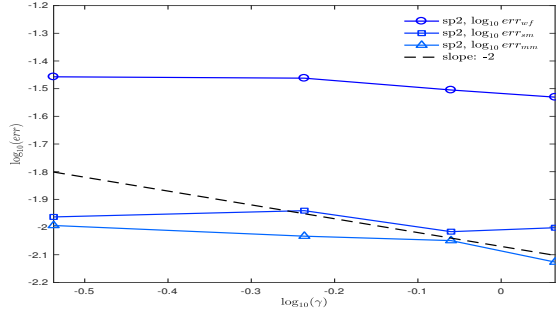
- (1) All of **sp1**, **sp2**, **wp** allow a longer time step Δt without loss of accuracy. By contrast, **sp0** performs well only when Δt is sufficiently small. The errors of **sp0** are almost proportional to Δt .
- (2) On the other hand, too small Δt leads to a dramatic increase in computational time. The running time of **sp0** is 86.00s for $\Delta t = 1\text{fs}$, 425.53s for $\Delta t = 0.1\text{fs}$, and 3738.89s for $\Delta t = 0.01\text{fs}$ on the computational platform: Intel(R) Core(TM) i7-6700 CPU (3.40GHz, 8MB Cache, 4 Cores, 8 Threads) and 16GB Memory (we use one thread for each task).

6 Conclusions and discussions

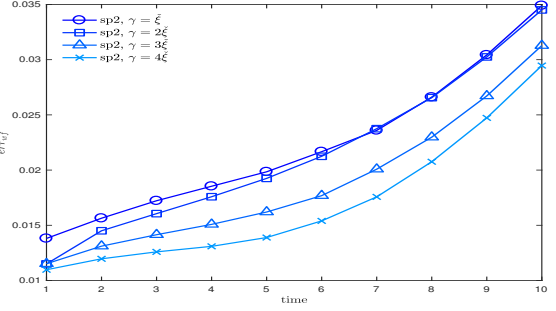
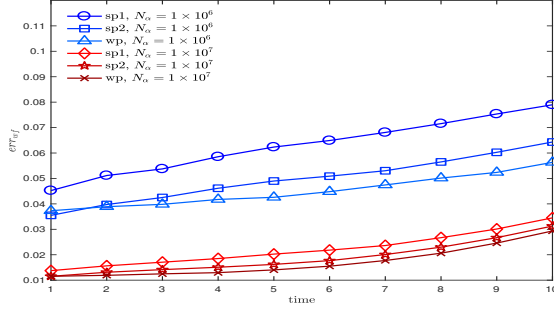
In this paper, we propose two efficient strategies to realize the signed-particle implementation of the Wigner branching random walk (WBRW). One is to interpret the multiplicative functional ξ/γ as the probability to generate new particles. The other is to employ a bootstrap filtering in the weighted-particle version. The numerical analysis on the bootstrap filtering, as well as the errors induced by resampling based on the uniform histogram, is given. Through detailed performance evaluations, we have shown the accuracy and efficiency of two proposed strategies, distinguished the differences of various approaches and uncovered the following facts.



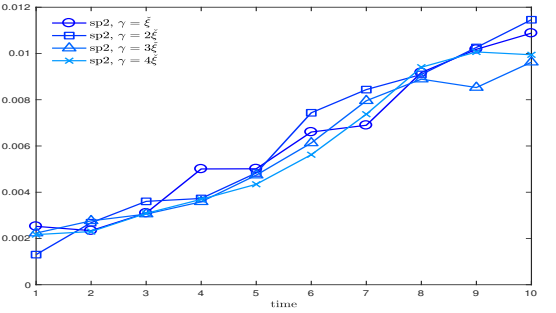
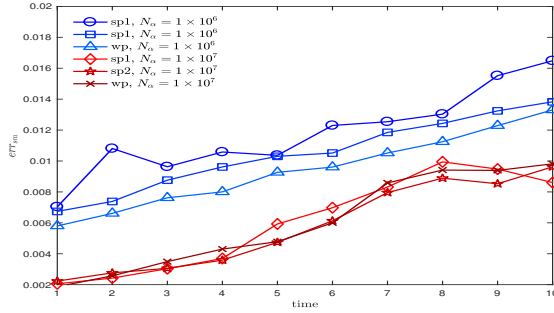
(a) Convergence rate with respect to N_α .



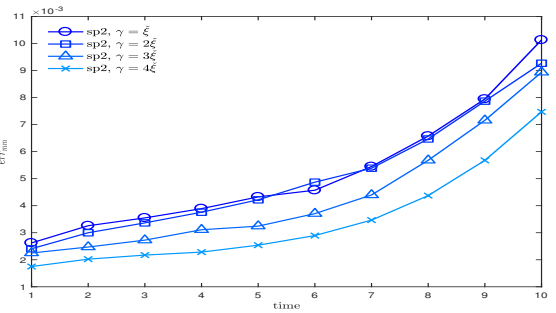
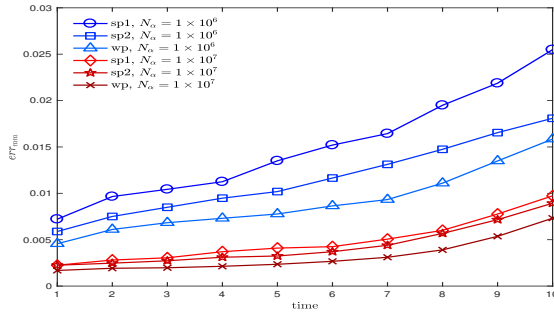
(b) Convergence rate with respect to γ .



(c) err_{wf} under different N_α (left) or different γ (right).



(d) err_{sm} under different N_α (left) or different γ (right).



(e) err_{mm} under different N_α (left) or different γ (right).

Figure 9: The 2D Gaussian scattering: Comparison among **sp2**, **sp1** and **wp**. **sp2** is slightly less accurate than the **wp** due to the random noises induced by the bootstrap filtering, but it is still better than **sp1**. **sp2** allows a reduction in variance as γ increases. Here we set the auxiliary function $\gamma = 3\xi$ and $T_A = 1fs$.

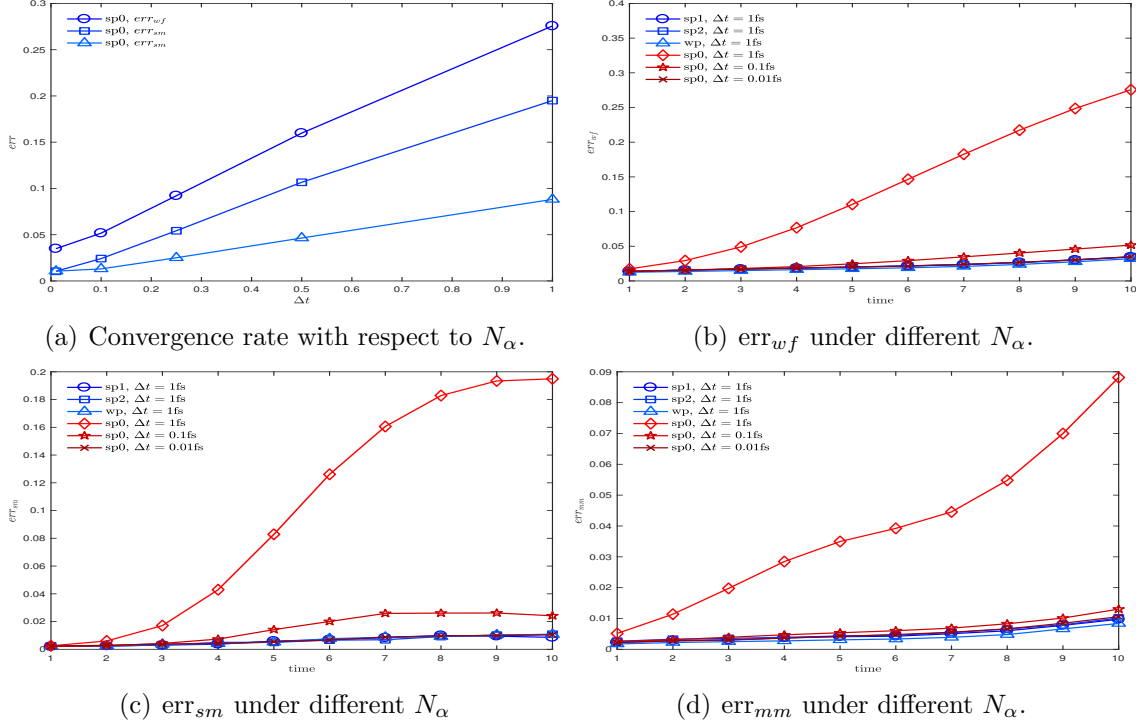


Figure 10: The 2D Gaussian scattering: Comparison among **sp0**, **sp1**, **sp2** and **wp**. **sp0** requires the time step Δt sufficiently small to ensure the accuracy, whereas **sp1**, **sp2** and **wp** alleviate such restriction. Here we set the auxiliary function $\gamma = \tilde{\xi}$ and $T_A = 1fs$.

- (1) WBRW implementation is more advantageous over the original signed-particle Wigner Monte Carlo method (**sp0**), since it alleviates the restriction on the time step. The accuracy of **sp2** and **wp** can be further improved by adjusting the auxiliary function γ .
- (2) Increasing the particle size N_α will systematically improve the accuracy, but the convergence order has some deviations from the theoretical order of $-1/2$ due to the deterministic errors induced by the resampling.
- (3) Both the accuracy and the growth of particle number of **sp1** is independent of γ . On the contrary, the **wp** is a variance reduction method and the choice of γ will give a systematic improvement on the accuracy with the order $\mathcal{O}(\gamma^{-2})$, at the cost of higher computational complexity.
- (4) The resampling procedure is indispensable for the consideration of not only efficiency but also accuracy. It helps to suppress both the exponential growth of particle number and the accumulation of stochastic errors. The resampling based on the uniform histogram performs quite well for $N_\alpha \geq N_h$. A balanced choice is $N_\alpha \approx 10N_h$. However, the efficiency of the resampling based on a uniform histogram is still undermined due to the curse of dimensionality.
- (5) **sp2** captures the merits of both **sp1** and **wp**, but introduces additional stochastic errors. It allows a variance reduction by increasing γ , and the histogram

can be stored and operated as integer-value matrices.

Towards a wider application of WBRW implementation of quantum mechanics, the resampling strategy should be improved to meet the challenge in higher dimensional problems, and some advanced statistical tools, such as the tree-based density estimation and the kernel density estimation [18], may be introduced.

Acknowledgement

This research was supported by grants from the National Natural Science Foundation of China (Nos. 11471025, 11421101).

Appendix

A. Proof of the Lemma 1

According to the first rule in Alg. 2,

$$\left| \frac{1}{N} \sum_{i=1}^N w_i \varphi(\mathbf{x}_i, \mathbf{k}_i) - \frac{1}{N} \sum_{i=1}^N \varphi(\tilde{\mathbf{x}}_i, \tilde{\mathbf{k}}_i) \right| = \left| \frac{1}{N} \sum_{i=1}^N r_i \varphi(\mathbf{x}_i, \mathbf{k}_i) - \frac{1}{N} \sum_{j=1}^{N_r} \varphi(\tilde{\mathbf{x}}'_j, \tilde{\mathbf{k}}'_j) \right|,$$

where $\tilde{\mathcal{S}} = \{(\tilde{\mathbf{x}}'_j, \tilde{\mathbf{k}}'_j)\}_{j=1}^{N_r}$ constitutes a subset that is randomly chosen from \mathcal{S} , and $r_i = w_i - k_i$. We allow $r_i = 0$ for some i .

Now we define S_N and \tilde{S}_N as

$$S_N = \sum_{i=1}^N r_i \cdot \frac{\varphi(\mathbf{x}_i, \mathbf{k}_i)}{N}, \quad \tilde{S}_N = \sum_{j=1}^{N_r} \frac{\varphi(\tilde{\mathbf{x}}'_j, \tilde{\mathbf{k}}'_j)}{N}.$$

It's easy to verify that \tilde{S}_N is unbiased ($\mathbb{E}\tilde{S}_N = S_N$) because

$$\begin{aligned} \mathbb{E}[\varphi(\tilde{\mathbf{x}}'_j, \tilde{\mathbf{k}}'_j)] &= \sum_{i=1}^N \Pr\{(\tilde{\mathbf{x}}'_j, \tilde{\mathbf{k}}'_j) = (\mathbf{x}_i, \mathbf{k}_i)\} \cdot \varphi(\mathbf{x}_i, \mathbf{k}_i) \\ &= \sum_{i=1}^N \frac{w_i - k_i}{\sum_{i=1}^N (w_i - k_i)} \cdot \varphi(\mathbf{x}_i, \mathbf{k}_i) = \sum_{i=1}^N \frac{r_i}{N_r} \cdot \varphi(\mathbf{x}_i, \mathbf{k}_i). \end{aligned}$$

According to the mutually independence of $(\mathbf{x}'_j, \mathbf{k}'_j)$ and the Cauchy-Schwarz inequality, it yields

$$\begin{aligned} \mathbb{E}|\tilde{S}_N - S_N|^2 &= \mathbb{E}|\tilde{S}_N - \mathbb{E}\tilde{S}_N|^2 = \frac{1}{N^2} \sum_{j=1}^{N_r} \mathbb{E} \left| \varphi(\mathbf{x}'_j, \mathbf{k}'_j) - \frac{1}{N_r} \sum_{i=1}^N r_i \cdot \varphi(\mathbf{x}_i, \mathbf{k}_i) \right|^2 \\ &\leq \frac{2}{N^2} \left[\sum_{j=1}^{N_r} \mathbb{E}|\varphi(\mathbf{x}'_j, \mathbf{k}'_j)|^2 + \left(\sum_{i=1}^N \frac{r_i}{N_r} \right)^2 \cdot \left(\sum_{i=1}^N |\varphi(\mathbf{x}_i, \mathbf{k}_i)| \right)^2 \right] \\ &\leq \frac{2(N_r + N)\|\varphi\|^2}{N^2} = \left(\frac{2N_r}{N^2} + \frac{2}{N} \right) \|\varphi\|^2. \end{aligned}$$

B. Proof of the Theorem 3

Let us consider the following function

$$A_j(\varphi)(\mathbf{x}_i, \mathbf{k}_i) = \varphi(\mathbf{x}_i, \mathbf{k}_i) - \frac{1}{\mu(\mathbf{D}_j)} \iint_{\mathbf{D}_j} \varphi(\mathbf{x}, \mathbf{k}) d\mathbf{x} d\mathbf{k}. \quad (\text{B.1})$$

Substituting Eq. (4.16) into Eq. (B.1), it yields

$$\begin{aligned} |A_j(\varphi)(\mathbf{x}_i, \mathbf{k}_i)| &\leq \frac{1}{\mu(\mathbf{D}_j)} \iint_{\mathbf{D}_j} |\varphi(\mathbf{x}, \mathbf{k}) - \varphi(\mathbf{x}_i, \mathbf{k}_i)| d\mathbf{x} d\mathbf{k} \\ &\leq \frac{1}{\mu(\mathbf{D}_j)} \iint_{\mathbf{D}_j} \|\varphi\|_{C^{0,\alpha}} \cdot \epsilon^\alpha d\mathbf{x} d\mathbf{k} = \|\varphi\|_{C^{0,\alpha}} \cdot \epsilon^\alpha. \end{aligned}$$

Then we arrive at

$$\begin{aligned} &|\langle \varphi, \frac{1}{N_\alpha} \sum_{i=1}^N w_i \delta_{\mathbf{x}_i, \mathbf{k}_i} \rangle - \langle \varphi, p_t \rangle| \\ &= \left| \frac{1}{N_\alpha} \sum_{i=1}^N \sum_{j=1}^{N_h} w_i \left[\varphi(\mathbf{x}_i, \mathbf{k}_i) - \frac{1}{\mu(\mathbf{D}_j)} \iint_{\mathbf{D}_j} \varphi(\mathbf{x}, \mathbf{k}) d\mathbf{x} d\mathbf{k} \right] \cdot \delta_{ij} \right| \\ &\leq \frac{1}{N_\alpha} \sum_{i=1}^N |w_i| \cdot \|\varphi\|_{C^{0,\alpha}} \cdot \epsilon^\alpha = (|\lambda^+| + |\lambda^-|) \cdot \|\varphi\|_{C^{0,\alpha}} \cdot \epsilon^\alpha, \end{aligned}$$

where δ_{ij} is given by

$$\delta_{ij} = \begin{cases} 1, & (\mathbf{x}_i, \mathbf{k}_i) \in \mathbf{D}_j, \\ 0, & (\mathbf{x}_i, \mathbf{k}_i) \notin \mathbf{D}_j. \end{cases}$$

For the second inequality, we start from

$$\begin{aligned} &\mathbb{E} \left| \langle \varphi, \frac{1}{N_\alpha} \sum_{i=1}^N w_i \cdot \delta_{\mathbf{x}_i, \mathbf{k}_i} \rangle - \langle \varphi, \tilde{p}_t \rangle \right|^2 \\ &\leq 2\mathbb{E} \left| \langle \varphi, \frac{1}{N_\alpha} \sum_{i=1}^N w_i \cdot \delta_{\mathbf{x}_i, \mathbf{k}_i} \rangle - \langle \varphi, \frac{\lambda^+}{N^+} \sum_{i=1}^{N^+} \delta_{\tilde{\mathbf{x}}_i^+, \tilde{\mathbf{k}}_i^+} + \frac{\lambda^-}{N^-} \sum_{i=1}^{N^-} \delta_{\tilde{\mathbf{x}}_i^-, \tilde{\mathbf{k}}_i^-} \rangle \right|^2 \\ &\quad + 2\mathbb{E} \left| \langle \varphi, \frac{\lambda^+}{N^+} \sum_{i=1}^{N^+} \delta_{\tilde{\mathbf{x}}_i^+, \tilde{\mathbf{k}}_i^+} + \frac{\lambda^-}{N^-} \sum_{i=1}^{N^-} \delta_{\tilde{\mathbf{x}}_i^-, \tilde{\mathbf{k}}_i^-} \rangle - \langle \varphi, \tilde{p}_t \rangle \right|^2. \end{aligned} \quad (\text{B.2})$$

The first term of Eq. (B.2) is bounded by Eq. (3.20), and the second term is bounded by Eq. (4.17).

References

- [1] E. Wigner. On the quantum corrections for thermodynamic equilibrium. *Phys. Rev.*, 40:749–759, 1932.

- [2] M. Nedjalkov, H. Kosina, S. Selberherr, C. Ringhofer, and D. K. Ferry. Unified particle approach to Wigner-Boltzmann transport in small semiconductor devices. *Phys. Rev. B*, 70:115319, 2004.
- [3] H. Kosina, M. Nedjalkov, and S. Selberherr. Theory of the Monte Carlo method for semiconductor device simulation. *IEEE Trans. Electron Devices*, 47:1898–1908, 2000.
- [4] J. M. Sellier, M. Nedjalkov, and I. Dimov. An introduction to applied quantum mechanics in the Wigner Monte Carlo formalism. *Phys. Rep.*, 577:1–34, 2015.
- [5] S. Shao and Y. Xiong. A computable branching random walk for the many-body Wigner quantum dynamics. *arXiv:1603.00159v2*, 2016.
- [6] R. Balescu. *Equilibrium and Nonequilibrium Statistical Mechanics*. John Wiley & Sons, New York, 1975.
- [7] V. I. Tatarskiĭ. The Wigner representation of quantum mechanics. *Sov. Phys. Usp*, 26:311–327, 1983.
- [8] W. Wagner. A random cloud model for the Wigner equation. *Kinet. Relat. Mod.*, 9:217–235, 2016.
- [9] J. M. Sellier, M. Nedjalkov, I. Dimov, and S. Selberherr. A benchmark study of the Wigner Monte-Carlo method. *Monte Carlo Methods Appl.*, 20:43–51, 2014.
- [10] S. Rjasanow and W. Wagner. A stochastic weighted particle method for the Boltzmann equation. *J. Comput. Phys.*, 124:243–253, 1996.
- [11] B. Yan and R. E. Caflisch. A Monte Carlo method with negative particles for coulomb collisions. *J. Comput. Phys.*, 298:711–740, 2015.
- [12] S. Shao and J. M. Sellier. Comparison of deterministic and stochastic methods for time-dependent Wigner simulations. *J. Comput. Phys.*, 300:167–185, 2015.
- [13] O. Muscato and W. Wagner. A class of stochastic algorithms for the Wigner equation. *SIAM J. Sci. Comput.*, 38:A1483–A1507, 2016.
- [14] H. Kosina, M. Nedjalkov, and S. Selberherr. Solution of the space-dependent Wigner equation using a particle model. *Monte Carlo Methods Appl.*, 10:359–368, 2004.
- [15] S. Shao, T. Lu, and W. Cai. Adaptive conservative cell average spectral element methods for transient Wigner equation in quantum transport. *Commun. Comput. Phys.*, 9:711–739, 2011.
- [16] Y. Xiong, Z. Chen, and S. Shao. An advective-spectral-mixed method for time-dependent many-body Wigner simulations. *SIAM J. Sci. Comput.*, 38:B491–B520, 2016.

- [17] L. Györfi. *Principles of Nonparametric Learning*. Springer-Verleg, Wien GmbH, 2002.
- [18] T. Hastie, R. Tibshirani, and J. Friedman. *The Elements of Statistical Learning: Data Mining, Inference, and Prediction*. Springer, New York, second edition, 2009.
- [19] J. S. Liu. *Monte Carlo Strategies in Scientific Computing*. Springer, New York, 2001.
- [20] N. Gordon A. Doucet, N. De Freitas. *An Introduction to Sequential Monte Carlo Methods. Sequential Monte Carlo Methods in Practice*. Springer-Verlag, New York, 2001.
- [21] M. Nedjalkov, P. Schwaha, S. Selberherr, J. M. Sellier, and D. Vasileska. Wigner quasi-particle attributes – An asymptotic perspective. *Appl. Phys. Lett.*, 102:163113, 2013.
- [22] P. Ellinghaus. *Two-Dimensional Wigner Monte Carlo Simulation for Time-Resolved Quantum Transport with Scattering*. PhD thesis, Institute for Microelectronics, TU Vienna, 2016.
- [23] C. P. Robert and G. Casella. *Monte Carlo Statistical Methods*. Springer, New York, second edition, 2004.
- [24] C. Vergé, C. Dubarry, P. Del Moral, and E. Moulines. On parallel implementation of sequential Monte Carlo methods: the island particle model. *Stat. Comput.*, 25:243–260, 2015.
- [25] T. E. Harris. *The Theory of Branching Processes*. Springer-Verlag, Berlin, 1963.